University of Iowa

Iowa Research Online

Theses and Dissertations

Summer 2017

Developing novel techniques for next generation rotating shield brachytherapy

Hossein Dadkhah
University of Iowa

Recommended Citation

Dadkhah, Hossein. "Developing novel techniques for next generation rotating shield brachytherapy." PhD (Doctor of Philosophy) thesis, University of Iowa, 2017.
https://doi.org/10.17077/etd.l03u-z0tg

DEVELOPING NOVEL TECHNIQUES FOR NEXT GENERATION ROTATING
SHIELD BRACHYTHERAPY

by

Hossein Dadkhah

A thesis submitted in partial fulfillment
of the requirements for the Doctor of Philosophy
degree in Biomedical Engineering in the
Graduate College of
The University of Iowa

August 2017

Thesis Supervisor: Associate Professor Ryan T. Flynn

Graduate College
The University of Iowa
Iowa City, Iowa

CERTIFICATE OF APPROVAL

_____

PH.D. THESIS

_____

This is to certify that the Ph.D. thesis of

Hossein Dadkhah

has been approved by the Examining Committee for
the thesis requirement for the Doctor of Philosophy degree
in Biomedical Engineering at the August 2017 graduation.

Thesis Committee: _____
                     Ryan T. Flynn, Thesis Supervisor

                     _____
                     Xiaodong Wu

                     _____
                     Sarah C. Vigmostad

                     _____
                     Edward Sander

                     _____
                     Weiyu Xu

                     _____
                     Joseph M. Reinhardt

To Hoda, my wife whose love is invaluable source of inspiration.

ACKNOWLEDGEMENTS

During the course of this work, the constant association with the members of our research team has been most pleasurable. Without their help and counsel, always generously and unstintingly given, the completion of this journey would have been immeasurably more difficult.

I would like to express my deepest gratitude toward my advisor, Dr. Ryan Flynn, whose passion for research, innovation, and education is only equaled by his passion for assisting others to live longer, healthier lives. He provided me with every bit of guidance, assistance, expertise, freedom, and encouragement during the course of this unrivaled experience. Besides, I was always inspired by his perpetual optimism even when things looked bleak, by his hard work and enduring professionalism even when it is not reciprocated, by his collegiality and scholarly generosity with his students and colleagues, and by his audacity in embarking on new research adventures. He has also been a constant source of support and encouragement in the development and implementation of my career goals.

There are many faculty and group members at the Department of Radiation Oncology, Department of Electrical and Computer Engineering, and Department of Biomedical Engineering at The University of Iowa who I wish to acknowledge. To Dr. Yusung Kim, for providing me with constructive and practical advice originated in his profound clinical and scientific background. To Professor Xiaodong Wu, for providing me and our team with the novel optimization and mathematical methods essential to treatment planning of the proposed approaches. To all the committee members, Drs. Joseph Reinhardt, Sarah Vigmostad, Edward Sander, Xiaodong Wu, Ryan Flynn, and Yusung

Kim, who were willing to participate in the three major exams toward my graduation and to offer suggestions and advices during this course. To all my previous and present colleagues and friends at our IMBT team, Xing Li, Yunlong Liu, Weiyu Xu, Myung Cho, Kaustubh Patwardhan, and Karolyn Hopfensperger for providing a friendly and cooperative atmosphere at our group and also useful feedback and insightful comments on my work.

Last but not least, a special debt of gratitude is due to my wife, Hoda, for all the dedication, patience, and support throughout the years. Her unwavering love, support, and encouragement were undeniably the bedrock upon which the past seven years of my life have been built. I also thank my parents, Ali and Mahin, for giving me the opportunity to live, learn, and love and for enabling me to follow my dreams.

ABSTRACT

Multi-helix rotating shield brachytherapy (RSBT) applicator and multi-source RSBT apparatus are two novel intensity-modulated brachytherapy techniques for the treatment of cervical and prostate cancer, respectively. The use of imaging techniques such as magnetic resonance imaging guided brachytherapy has enabled the precise identification and contouring of tumor volumes for treatment planning, as well as demonstrated the challenges associated with using conventional high dose rate brachytherapy (HDR-BT) approaches to conform the radiation dose to the target and avoid surrounding sensitive healthy tissues. The target conformity of conventional HDR-BT dose distributions is restricted based on the geometrical constraints imposed by the position and shape of the tube-shaped applicators, as well as the radially-symmetric radiation dose distributions produced by the radiation sources. Dose distribution conformity for cervical and prostate cancer can be significantly improved relative to conventional HDR-BT through the use of multi-helix and multi-source RSBT techniques, respectively. In this study, two novel RSBT concepts for treating cervical and prostate cancer were introduced and the dosimetric impact was evaluated.

A Henschke-type cervical cancer applicator, designed for an electronic brachytherapy (eBx) source (Xoft Axxent^{TM}) and a 0.5 mm thick tungsten partial shield with 180˚ or 45˚ azimuthal emission angles, is proposed. The interior wall of the applicator contains six evenly-spaced helical keyways that rigidly define the emission direction of the partial radiation shield as a function of depth in the applicator. The shield contains three uniformly-distributed protruding keys on its exterior wall and is attached to the source such that it rotates freely, thus longitudinal translational motion of the source

is transferred to rotational motion of the shield. RSBT treatment plans were generated for five cervical cancer patients with a diverse range of high-risk target volume (HR-CTV) shapes and applicator positions. Treatment delivery time and tumor coverage (D_{90} of HR-CTV) were the two metrics used as the basis for evaluation and comparison.

With multi-source RSBT apparatus, precise angular and linear positioning of partially-shielded ^{153}Gd brachytherapy sources in interstitial needles for the treatment of locally-advanced prostate cancer is carried out. Following needle implantation through the patient template, an angular drive mechanism is docked to the patient template. Each needle is coupled to a multisource afterloader catheter by a connector passing through a shaft. The shafts are rotated about their axes by translating a moving template between two stationary templates. Shafts' surfaces and moving template holes are helically threaded with the same pattern such that translation of the moving template causes simultaneous rotation of the shafts. The catheter angles are simultaneously incremented throughout treatment. For each rotation angle, source depth in each needle is controlled by a multisource afterloader, which is proposed as an array of belt-driven linear actuators, each of which drives a wire that controls catheter depth in a needle.

In conclusion, the helical RSBT approach for treating cervical cancer and the multi-catheter RSBT approach for treating prostate cancer, powered with novel radiation sources amenable to shielding, are clinically- and mechanically-feasible techniques that dosimetrically outperform conventional brachytherapy methods while minimizing damage to healthy tissues inside and/or adjacent to the target.

PUBLIC ABSTRACT

Brachytherapy is a widely-used form of radiotherapy where a radiation source is placed inside or next to the tumor region. Conventional brachytherapy approaches are either non-conformal to the tumor volume or invasive to the healthy tissues surrounding the tumor. In the current study, two novel brachytherapy mechanisms were proposed as clinically-feasible alternatives to conventional brachytherapy techniques for treating cervical and prostate cancer. In the first part of this work, an innovative brachytherapy approach for treating cervical cancer is put forward. The goal is to deliver a high radiation dose to tumor, which covers almost the whole tumor volume, while still keeps the radiation dose delivered to the healthy organs adjacent to the tumor (bladder, rectum, and sigmoid colon) lower than the standard. In the second part of this work, an innovative brachytherapy mechanism for treating locally-advanced prostate cancer is proposed with the objective of delivering lower radiation dose to surrounding normal structures, urethra in particular, and increasing the radiation dose delivered to the prostate.

TABLE OF CONTENTS

LIST OF TABLES

LIST OF FIGURES

xiv

NOMENCLATURE

3-D	Three dimensional
AJCC	American Joint Committee on Cancer
BT	Brachytherapy
CT	Computed tomography
DMBT	Direction modulated brachytherapy
DVH	Dose volume histogram
EBRT	External beam radiation therapy
eBx	Electronic brachytherapy
EQD2	Equivalent dose as given in 2 Gy-fractions
FIGO	Féderation Internationale de Gynécologie et d'Obstétrique
GEC-ESTRO	The Groupe Européen de Curiethérapie and the European SocieTy for Radiotherapy & Oncology
GTV	Gross tumor volume
HDR-BT	High dose rate brachytherapy
HPV	Human papillomavirus
HR-CTV	High risk clinical target volume
H-RSBT	Multi-helix rotating shield brachytherapy
ICBT	Intracavitary brachytherapy
IMBT	Intensity modulated brachytherapy
I-RSBT	Interstitial rotating shield brachytherapy
IS+ICBT	Interstitial plus intracavitary brachytherapy

MR	Magnetic resonance
OAR	Organ at risk
RSBT	Rotating shield brachytherapy
S-RSBT	Serial rotating shield brachytherapy
TNM	Tumor, node, and metastases

Part I. MULTI-HELIX ROTATING SHIELD BRACHYTHERAPY FOR CERVICAL CANCER[1]

---

1 INTRODUCTION

1.1 Cervical cancer

Cervical cancer is a malignant neoplasm that forms in the tissues of the cervix uteri, the organ connecting the uterus and vagina. It is the 4th most widespread cancer in women throughout the world following breast, colorectal, and lung cancers, with an approximate assessment of 528,000 new cases in 2012.[1] With around 266,000 deaths in 2012, it is, additionally, considered as the fourth cause of female cancer morbidity globally. In addition, in the U.S. it is the third most common gynecological cancer while in developing countries it is the leading cause of cancer mortality in women.[2] Those patients with postcoital or unaccountable abnormal vaginal bleeding, pelvic pain, atypical discharge, or a perceptible lesion are remarkably susceptible to this type of cancer and highly recommended for comprehensive evaluations.[3]

The underlying cause of cervical cancer is some types of chronic human papillomavirus (HPV) infection which is a productive infection triggered in keratinocytes of the skin or mucous membranes.[4] Other factors including smoking, chlamydia infection, unhealthy diets, birth control pills, multiple pregnancies, and family history can play a key role in forming a malignant cervical tumor.[5] The 33% death rate (beyond 4,200 cases out of all new cervical cancer cases in 2011) is associated with this type of gynecological cancer in the U.S.[6] Table 1[2, 7] shows The American Joint Committee on Cancer (AJCC) TNM (Tumor, node, and metastases) classification and the Féderation Internationale de Gynécologie et d'Obstétrique (FIGO) staging system for cervical cancer as well as local control and survival rates associated with each stage and classification.

2

Table 1: Cervical cancer categories and staging with local control and survival rate.

TNM Categories	FIGO Stages	Surgical-Pathologic findings	Local control rate	Survival rate
TX		Primary tumor cannot be assessed		
T0		No evidence of primary tumor		
Tis		Carcinoma in situ (preinvasive carcinoma)		
T1	I	Cervical carcinoma confined to the cervix		
T1a	IA	Invasive carcinoma diagnosed only by microscopy	95-100%	95-100%
T1a1	IA1	Measured stromal invasion ≤ 3.0 mm in depth	95-100%	
T1a2	IA2	Measured stromal invasion > 3.0 mm in depth	95-100%	
T1b	IB	Clinically visible lesion confined to the cervix		
T1b1	IB1	Clinically visible lesion ≤ 4.0 cm in greatest dimension	90-95%	85-90%
T1b2	IB2	Clinically visible lesion > 4.0 cm in greatest dimension	60-80%	60-70%
T2	II	Cervical carcinoma invades beyond uterus but not to pelvic wall or to lower third of vagina		
T2a	IIA	Tumor without parametrial invasion	80-85%	75%
T2a1	IIA1	Clinically visible lesion ≤ 4.0 cm in greatest dimension		

Table 1—continued

T2a2	IIA2	Clinically visible lesion > 4.0 cm in greatest dimension		
T2b	IIB	Tumor with parametrial invasion	60-80%	60-65%
T3	III	Tumor extends to pelvic wall		
T3a	IIIA	Tumor involves lower third of vagina, no extension to pelvic wall	60%	25-50%
T3b	IIIB	Tumor extends to pelvic wall and/or causes hydronephrosis or nonfunctional kidney	50-60%	25-50%
T4	IV	Tumor invades mucosa of bladder or rectum and/or extends beyond true pelvis		
T4a	IVA	Tumor invades mucosa of bladder or rectum	30%	15-30%
T4b	IVB	Tumor extends beyond true pelvis		<10%

Cervical cancer tumors with stages ranging from IB1 to IVB are conventionally considered as the advanced or malignant cases, due to their bulky volumes which are normally greater than 40 cm^3. Brachytherapy (BT) is considered as an inevitable component of the treatment for stages more invasive than IB. As indicated in Table 1, in stage IB2 the tumor is laterally extended larger than 4 cm and is confined to the cervix boundaries while in an invasive stage such as IVA, cancer extended over nearby organs, such as the bladder or rectum. Cervix and endometrium are among those tissues in a woman body that can receive high radiation doses with minimal sequelae. This specification accounts for the potential to treat endometrial and cervical cancer with high external and brachytherapy dose. Although cervix has such a capability, combined

4

internal and external radiation therapy has some late effects including vaginal shortening associated with fibrosis and loss of elasticity and lubrication.[8]

1.2 Standard care for locally-advanced cervical cancer

Retrospective experimental analyses suggest that patients with bulky stage IB tumors are more responsive to concomitant treatment with cisplatin and radiation therapy than to radiation therapy solely or even to other regimens in which radiation therapy is included but cisplatin is not.[9] Patients with locally-advanced cervical cancer typically receive external beam radiation therapy (EBRT) with concurrent chemotherapy followed by high dose rate brachytherapy (HDR-BT) to the tumor site.[10] The combination of treatment modalities of EBRT, chemotherapy, and magnetic resonance (MR) image guided intracavitary brachytherapy with supplemental interstitial brachytherapy for patients with laterally-extended non-symmetric bulky tumors of greater than 40 cm^3 has been demonstrated to be much more effective than either of these treatment modalities alone.[11]

1.3 Cervical cancer brachytherapy

The treatment outcome of regimens with BT shows improvement in terms of both cancer recurrence rates and survival rates.[12, 13] Conventional intracavitary brachytherapy (ICBT) for cervical cancer, as shown in **Figure 1**,[14] is delivered by means of a small high-energy radioactive source passing through a curved applicator which is placed into the uterus and vagina of the patient.

5
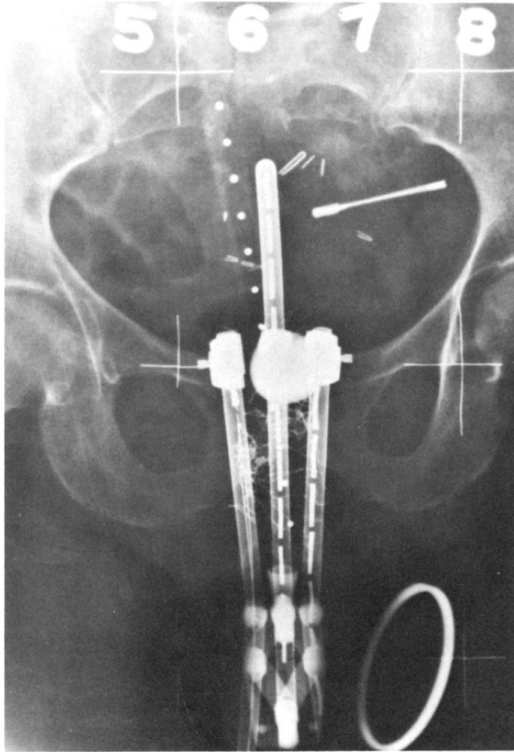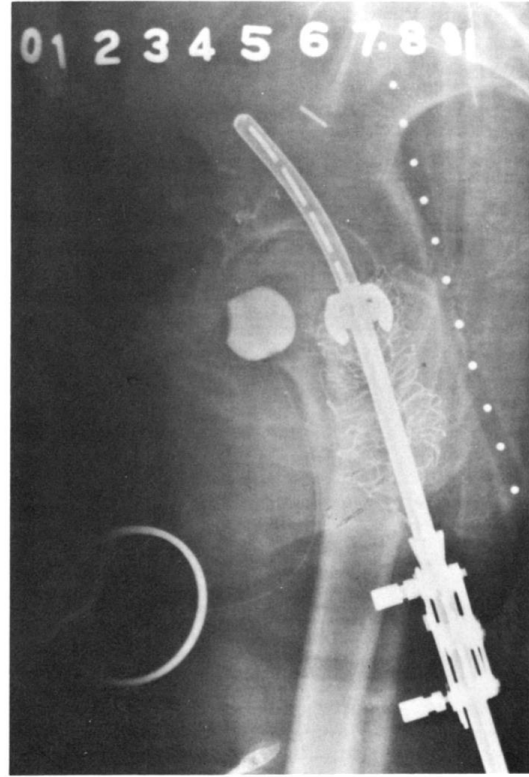
(a)   **(b)**

Figure 1: Localization radiographs of an ICBT Henschke-type applicator in (a) anterior-posterior and (b) lateral positions.

Conventional ICBT may not deliver sufficient radiation dose, particularly in cases with advanced cervical cancer or in cases that are distorted anatomically. Such cases are usually showing high incidence of local failure and some complications. Interstitial brachytherapy can be a potentially effective alternative for conventional ICBT in such cases.[15] Interstitial brachytherapy is potentially capable of delivering a curative dose to tumors that are positioned far from an accessible anatomic cavity. These tumors normally extend beyond the range of the tandem-ovoid applicator.[16] In this approach several interstitial needles used to provide anatomical access so that the radiation sources can be positioned within and around the target volume.

6

Combined interstitial BT and conventional ICBT (IS+ICBT) in conjunction with MRI-based treatment planning was first introduced by Kiristis et al in 2006.[17] A modified ring applicator (**Figure 2**), named Vienna applicator, facilitates interstitial needles to be positioned aligned with the conventional intrauterine applicator. This method is leading to increase in target coverage, treated volume, and total dose without compromising organ at risk (OAR) sparing.

Figure 2: Vienna applicator: a modified ring applicator for IS+ICBT. Needles are hollow metal tubes which are inserted through holes in the ring.

1.3.1 Challenges with the current BT approaches

The combination of treatment modalities of EBRT, chemotherapy, and MR image guided IS+ICBT for patients with laterally-extended non-symmetric bulky tumors of greater than 40 cm^3 has been demonstrated to be much more effective than either of these treatment modalities alone.[11] Introducing intraoperative MR image guidance into BT treatment planning of cervical cancer reduced the overestimation of the high risk clinical target volume (HR-CTV) (using GEC-ESTRO guidelines)[18] caused by the inherent lack

of precision in the images from computed tomography (CT).[19] Therefore clinicians are equipped with the means to accurately contour the regions of interest. IS+ICBT (the Vienna applicator) is proposed as a way to achieve more HR-CTV conformal dose distributions[17, 20] since ICBT alone has been shown to be incapable of delivering adequate doses to the tumor,[21-23] leading to suboptimal local control and survival. The IS+ICBT procedure reduces tumor underdose, but it demands supplementary needles for interstitial ^{192}Ir BT placement, and requires a shielded BT suite and additional MRI imaging.[24-27] The delivery time is also increased relative to ICBT by a factor of between five and eight.[22] Another major challenge to clinical implementation of IS+ICBT approach is that few physicians are familiar with its delivery and it is more invasive than ICBT alone, as the interstitial needles in this technique are generally associated with undesired bleeding. In addition, the deliverable and attainable dose escalation with ICBT alone is adversely affected by the OARs adjacent to the HR-CTV (bladder, rectum, and sigmoid colon)[28-30] as well as the emission of radially-symmetric dose distributions around the BT source that is constrained to travel through a prespecified channel (the intracavitary applicator).

However, pelvic control (cervix, uterine corpus, vagina, parametric, and lymph nodes) with IS+ICBT technique is 90% at 3 years in the absence of any increase in mortality, while pelvic control was 63% prior to the introduction of the Vienna series applicators.[11] This followed the introduction of MR-enabled IS+ICBT dose escalation to the high-risk clinical target volume (HR-CTV) using GEC-ESTRO guidelines,[18] simultaneous cisplatin chemotherapy, and laparoscopic pelvic node dissection with macroscopic removal for the majority of the patients in the most recent series. Although it is unclear what percentage of the observed improvement in pelvic control is attributable

8

to the use of MR-enabled IS+ICBT alone, there is little doubt that the resulting dose escalation played an important role in obtaining such positive results. For patients with smaller residual tumors (<5 cm), the advantage of the IS+ICBT approach is reduced as obtaining HR-CTV tumor dose conformity with ICBT is possible.

1.3.2 Intensity modulated brachytherapy

The tumor conformity and achievable dose escalation as well as the sensitive structure sparing capability of conventional HDR-BT dose distributions are limited based on the geometrical constraints imposed by the position and shape of the applicators or catheters, as well as the spatial symmetry of the dose distributions produced by conventional unshielded BT sources. Dose distribution conformity and sensitive healthy tissue avoidance can be considerably improved through the use of intensity modulated brachytherapy (IMBT) in conjunction with a specific radiation source amenable to shielding.

Potential alternatives to IS+ICBT for cervical cancer that would be dosimetrically superior to ICBT alone have been proposed, including rotating shield brachytherapy (RSBT)[31-35] and direction-modulated brachytherapy (DMBT).[36, 37] With RSBT as proposed for cervical cancer,[31-35] an electronic brachytherapy (eBx) source (Xoft AxxentTM, iCAD, Inc., Nashua, NH, USA) with a rotating partial shield travels down an intracavitary applicator, and the amount of radiation delivered in a given direction is modulated by controlling the amount of time the aperture created by the shield points in a that direction. With DMBT for cervical cancer (**Figure 3**),[36, 37] a multi-channel applicator with an MR-compatible, photon-attenuating tungsten core is proposed, and the directional

modulation is achieved by controlling the dwell time of the ^{192}Ir radiation source at each dwell position.
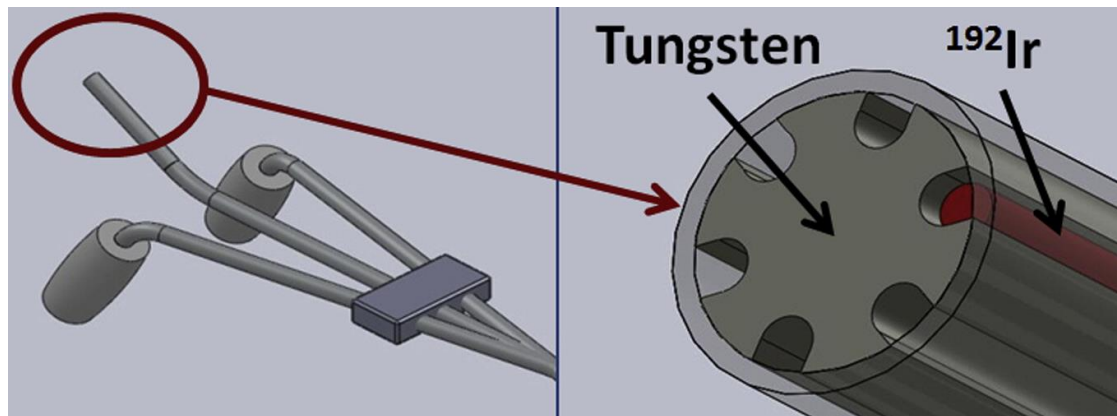
Figure 3: The DMBT tandem design with six evenly-spaced peripheral channels. Due to the shielding capability of the core, which is made out of a tungsten alloy, the HDR-BT source is shooting the radiation only into the direction of the channel's window.

1.4 Objectives of the PhD project

Our long-term objective in the current project was to improve the treatment of locally-advanced cervical cancer by developing a mechanically- and clinically-feasible RSBT technique, named multi-helix RSBT (H-RSBT). With H-RSBT, only linear translational motion of the radiation source/shield combination is necessary for the delivery, simplifying the process relative to previously proposed RSBT ideas.[31, 32, 35] In one of the previous studies[32] it was demonstrated that serial RSBT (S-RSBT), in which the partial shield is rotated to 16 angular positions at each 5-mm-spaced dwell position, has the potential to provide equivalent or superior HR-CTV D_{90}-values comparable to those of IS+ICBT for a range of different HR-CTV shapes and applicator positions, under the same OAR constraints to the bladder, rectum, and sigmoid colon. However, the authors have been unsuccessful at developing an S-RSBT system that has the potential to

10

operate safely with curved applicators due to the mechanical challenge of accurately rotating a radiation shield about a fixed dwell position inside a curved applicator. The H-RSBT technique, in which the partial shield is rotated to 6 angular positions at each 1.7-mm-spaced dwell position, is designed to overcome the obstacles to S-RSBT implementation, enabling the delivery of deliberately non-symmetric, tumor-conformal, dose distributions that would be impossible to deliver with conventional, unshielded, radiation sources in intracavitary applicators.

1.5 Innovation of the proposed technique

The innovative potential of this project is characterized by a number of unique features which originate in a coherent and well-established framework for RSBT delivery of cervical cancer that have been developed through the years, deserving attention from both theoretical and clinical perspectives. The primary aim of the present study is to adopt the concept of RSBT for cervical cancer with the emphasis on developing mechanically and clinically reliable novel technique and tangible system.

Cervical cancer patients with locally advanced disease typically receive the brachytherapy boost using one of the commercially available MRI-compatible intracavitary applicators,[10] none of which are straight in shape due to the complicated shape of the uterine cervix. Therefore the major challenge associated with implementing RSBT for cervical cancer is the simultaneous rotation and translation of the shielded source inside a small-diameter applicator part of which is curved. H-RSBT technique[34] is a mechanically feasible solution envisioned to surmount that obstacle. H-RSBT enables cervical cancer RSBT delivery using solely longitudinal and translational motion of the source and shield combination, tackling the challenges associated with previously

11

proposed RSBT method[32] based on a serial (S-RSBT) step-and-shoot delivery technique, which required independent translational and rotational motion. Applying RSBT in cervical cancer treatment procedures leads to a tangible improvement in achieving the tumor conformal dose distributions.

2 METHODS

2.1 Brachytherapy source

A partially shielded Xoft Axxent^{TM} eBx source[38] is considered as the brachytherapy source, which is a miniature x-ray source that is sheathed in a 5.4 mm diameter water-cooled catheter. The tube can be operated between 20 and 50 kVp, at a standard operating voltage of 50 kV and tube current of 300 μA. The air-kerma strength of an eBx source is 1.4 kGy/h. The eBx source is driven by a remote afterloading device (control console), which is a robotic arm that can control the location of the source inside the applicator to better than ±1 mm resulting in providing the desired longitudinal translation. The controller unit is also equipped with a pullback arm which has three adjustable joints allowing a desired longitudinal translation and better positioning and alignment of the source through a channel or applicator in order to provide a proper-shaped dose distribution.

2.2 Applicator and shield design

A novel applicator/shield/source system (**Figure 4**) with an outer diameter of 9.4 mm was designed to enable RSBT dose delivery for cervical cancer. Based on H-RSBT technique, the direction of a partial radiation shield is controlled using only translational motion of the radiation source. This is an advantageous property, as the eBx system already provides accurate translational motion capability, enabling the system to be extended to accommodate RSBT delivery without the addition of rotational motors, simplifying the implementation process.
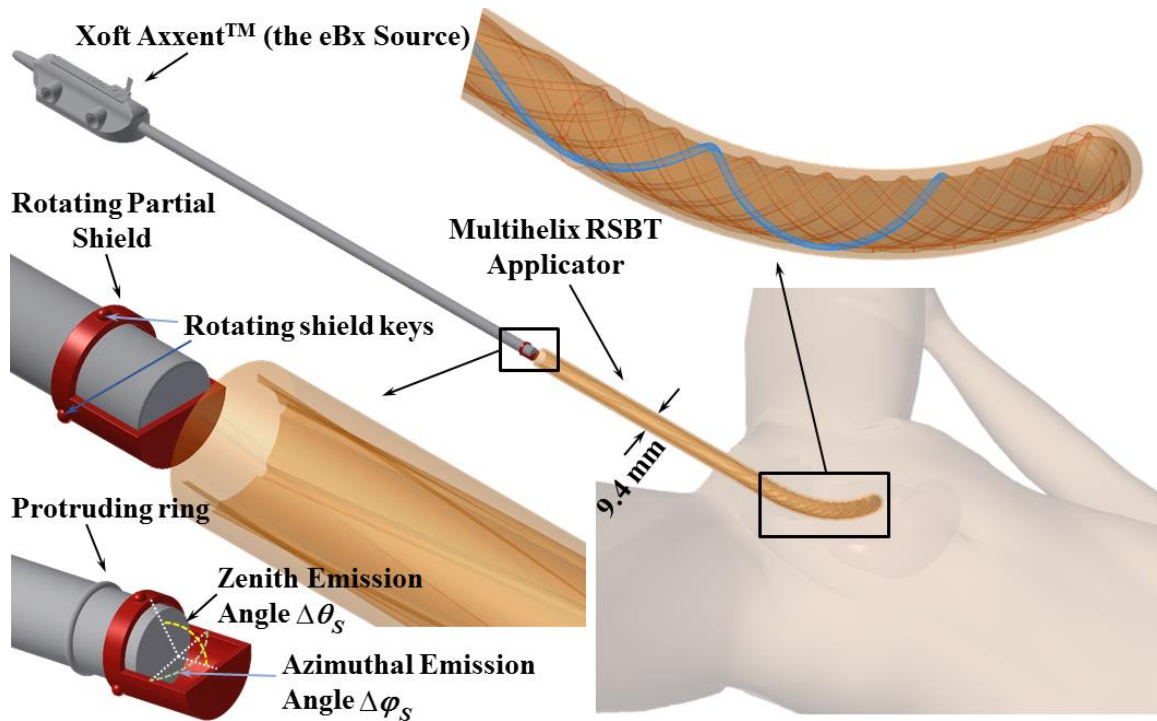
Figure 4: Multi-helix rotating shield brachytherapy (H-RSBT) system design.

The common applicator shape for cervical cancer brachytherapy, shown in **Figure 4**, has a curved central (tandem) applicator that can be substituted for tandem applicators with different curvatures depending on the patient and day. The H-RSBT applicator is an intracavitary tandem-type intrauterine applicator that is inserted past the cervix and into the patient's uterus. It contains six evenly-spaced helical keyways, which provide pathways that the keys from the shield follow when the source is translated. The rotating shield attaches to the end of the eBx catheter and rotates freely about the catheter inside the applicator. The shield has three uniformly-distributed protruding keys on its exterior wall, which occupy three of those six keyways at a given time. The position of the source in the applicator dictates the direction of the radiation shield and therefore the irradiation direction, thus H-RSBT only requires translational motion of the BT source inside the applicator for the shield to rotate. Since the clinical eBx unit already has a translational

drive, no additional motors would be needed to deliver H-RSBT. The keyways, as shown in **Figure 4**, start at the proximal entrance to the straight part of the applicator with a loose pitch (15 cm per rotation) that increases linearly to the desired pitch (3.33 cm per rotation) at the curved part of the applicator. This approach enables a smooth mechanical transition of the shield from the straight to the curved part of the applicator.
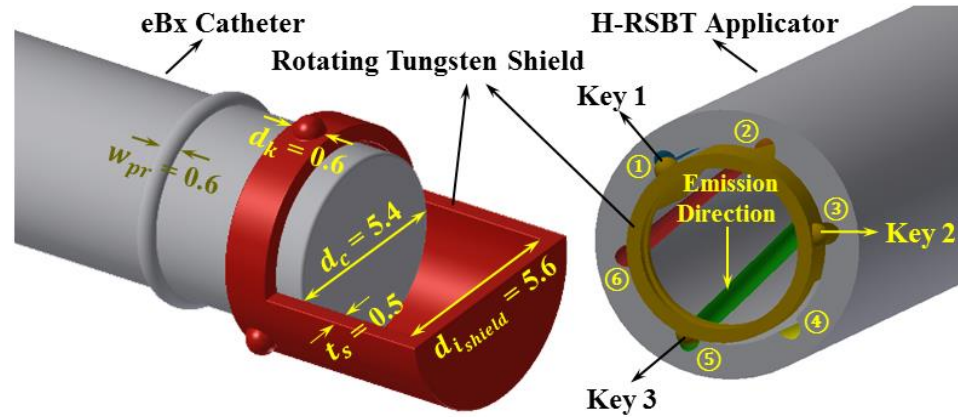
Figure 5: Cross section of H-RSBT applicator and shield. All dimensions are in mm.

An important feature of the H-RSBT applicator shown in **Figure 4** is that it contains six loosely-wound helical keyways that are longitudinally offset from each other. A cross section of the applicator is shown in **Figure 5**. Multiple keyways are required when they are loosely wound since using only a single keyway would not provide enough emission angles per unit applicator length to deliver dose distributions that are competitive with S-RSBT. Having six keyways increases the number of shield emission angles per cm, enabling an improvement in the deliverable dose distributions. By setting source travel per rotation of the keyways to 3.33 cm, H-RSBT dose distributions have the potential to be equivalent to S-RSBT dose distributions, as the number of emission angles per cm for H-RSBT is approximately the same as that for S-RSBT. Thus H-RSBT and S-

RSBT create 36.6 and 35.4 emission angles per cm of source travel inside the patient, respectively.

Clinical H-RSBT delivery would proceed as follows. The entire H-RSBT delivery would be done using one or more shields each with three protruding keys attached on its surface. For the first (of six) delivery segments, the shield keys #1, # 2, and #3 would occupy keyways #1, #3, and #5, respectively, as shown in **Figure 5**. The source would travel to the distal end of the applicator, stopping along the way at discrete longitudinal/angular dwell positions for preset dwell times. After the first segment, the source and shield could be retracted and re-inserted with the shield keys occupying a second combination of keyways, which would be keyways #2, #4, and #6, respectively. This proceeds until all of the desired combinations of keyways have been used for the delivery.

The shield used in the H-RSBT system must rotate about the radiation source smoothly and unimpeded during the dose delivery procedure. Therefore a connection between the shield and the water cooling catheter surrounding the eBx source is needed. As shown in **Figure 4**, in order to attach the shield to the eBx catheter such that it rotates freely, it is proposed to re-manufacture the cooling catheter such that it has a protruding circumferential plastic ring that can be used to hold the shield in place. Further, as shown in **Figure 5**, the tungsten shield thickness is 500 microns, which is enough to provide less than 0.1% dose transmission, while still rotating freely about the water cooling catheter. As the partially shielded cylinder is not curved and will remain a straight cylinder through the whole procedure, the inner diameter of the applicator is restricted in terms of the magnitude of both length and thickness of the shield.

16

2.3 Source trajectory and shield emission direction

A Henschke style applicator can be modeled as a straight tube and an attached arc with a radius of curvature of R_c. **Figure 6(a)** and **Figure 6(b)** show the geometrical parameters of a single helical keyway on a single dwell position in global and local coordinate systems, respectively. According to it, assume the following: R_I is the interior radius of the applicator, $\vec{h}(\ell)$ is applicator axis located in 3-D space at position ℓ along the applicator axis, $\alpha_m(\ell)$ is angle of the keyway m at position ℓ in the applicator while $m = 1, 2, \ldots, 6$, ℓ_r is the source travel per one rotation of a keyway inside the curved part of the applicator, and $\vec{p}_m(\ell)$ is the 3-D spatial location of the center of the entrance to the keyway m at position ℓ along the applicator. In general, the location of the entrance to keyway m at position ℓ is:

$$\vec{p}_m(\ell) = \vec{h}(\ell) + \vec{q}_m(\ell),$$
(1)

where $\vec{q}_m(\ell)$ is the vector between the applicator axis at position ℓ and the inner applicator wall at keyway m, defined in the $(\hat{x}, \hat{y}, \hat{z})$ coordinate system (**Figure 6(b)**) as:

$$\vec{q}_m(\ell) = R_I \cos[\alpha_m(\ell)]\hat{x}(\ell) + R_I \sin[\alpha_m(\ell)]\hat{y}(\ell),$$
(2)

and $\alpha_m(\ell)$ is defined as:

$$\alpha_m(\ell) = \pi \left(\frac{m-1}{6} + \frac{2\ell}{\ell_r} \right).$$
(3)

Thus $\vec{p}_m(\ell)$ is calculated as:

$$\vec{p}_m(\ell) = \{R_I \cos[\alpha_m(\ell)]\}\hat{x} + \left\{ R_c \left[1 - \cos\left(\frac{\ell}{R_c}\right) \right] + R_I \cos\left(\frac{\ell}{R_c}\right) \sin[\alpha_m(\ell)] \right\}\hat{y}$$

$$+ \left\{ R_c \sin\left(\frac{\ell}{R_c}\right) - R_I \sin\left(\frac{\ell}{R_c}\right) \sin[\alpha_m(\ell)] \right\}\hat{z}.$$
(4)

17
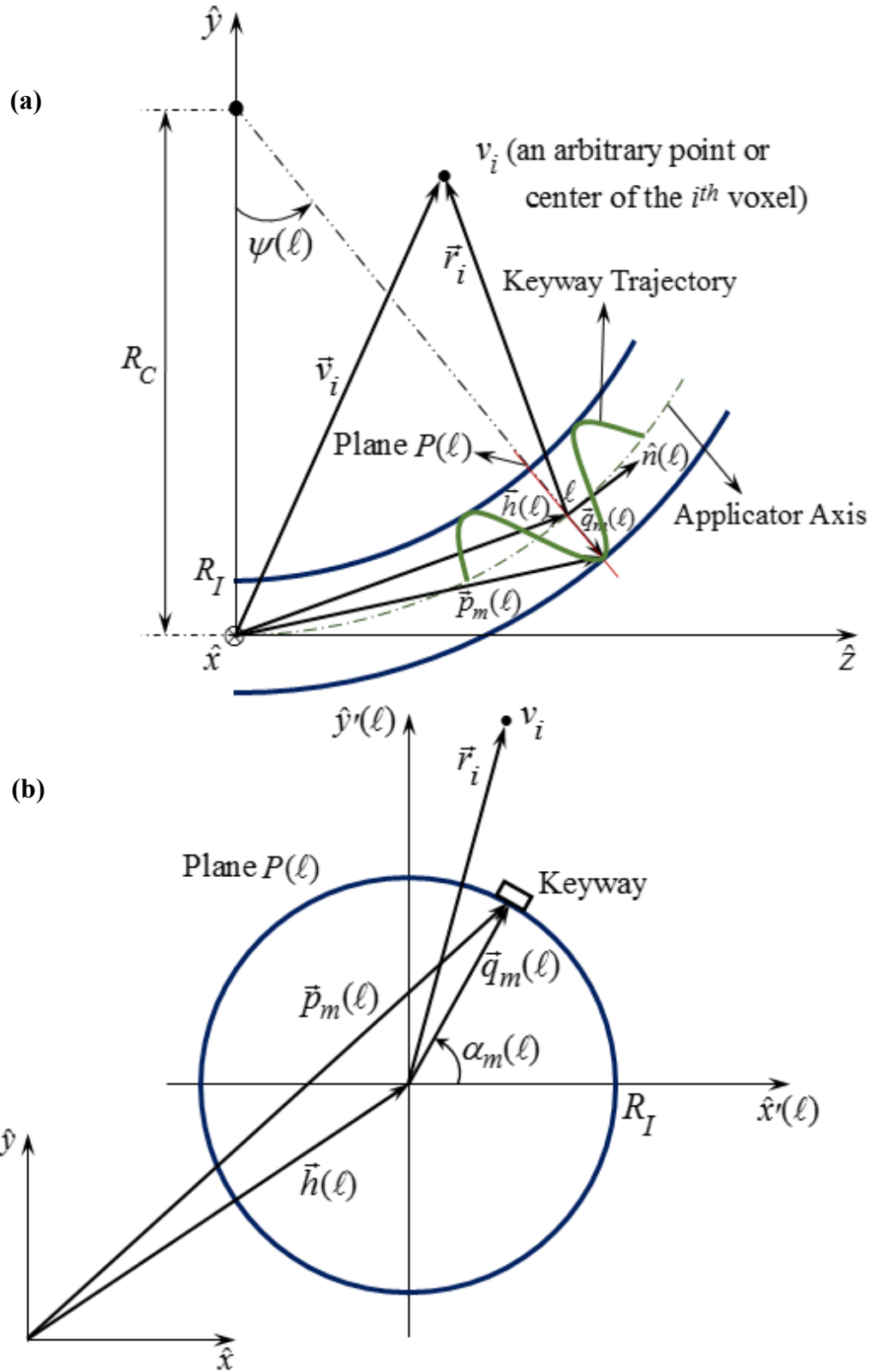
Figure 6: H-RSBT trajectory geometry and related parameters and coordinate systems.

2.4 Patients and dose prescription

Five patients with cervical cancer staging from IB to IVA were considered in an Institutional Review Board approved study. As shown in **Table 2** HR-CTV volumes ranged from 42.2 to 98.8 cm^3 (mean 68.1 cm^3, standard deviation 23.8 cm^3) and HR-CTV extents ranged from 6.3 to 9.6 cm (mean 7.9 cm, standard deviation of 1.8 cm). All the CTVs and OARs were manually contoured by physicians on T2-weighted 1 mm $\times$ 1 mm $\times$ 3 mm-resolution MR images taken with a Siemens MAGNETOM 3T scanner (Siemens, Germany) at the beginning of the first fraction of brachytherapy. A titanium Fletcher-Suit-Delclos style tandem and ovoids (Varian Medical Systems, Palo Alto, CA) was used as the brachytherapy applicator. The same datasets were used for the current study as by Yang et al (2013).[32]

Table 2: High-risk clinical target volume (HR-CTV) volumes and dimensions for all patients considered.

	HR-CTV Volume (cm^3)	HR-CTV Maximum Dimension (cm)
Patient #1	42.2	6.3
Patient #2	45.8	7.4
Patient #3	78.0	8.6
Patient #4	98.8	9.6
Patient #5	75.0	7.5
Average	68.0	7.9
Standard Deviation	23.8	1.8
Range	[42.2 98.8]	[6.3 9.6]

All patients received external beam radiation therapy in 25 fractions at 1.8 Gy per fraction. It was assumed for all the cases that the external beam radiotherapy dose was

19

uniformly delivered in the HR-CTV and OARs. The dose in each voxel was converted to equivalent dose as given in 2 Gy-fractions (EQD2) using the linear quadratic model[39] where the linear-quadratic parameter, α/β, set to 3 Gy for the OARs and 10 Gy for the HR-CTV.

Based on the institutional standard at The University of Iowa, the BT dose was simulated to be delivered over five fractions. For all the generated BT treatment plans the EQD2 of the HR-CTV was escalated until the EQD2 D_{2cc} tolerance of any of the three OARs was reached. The OAR's tolerances were in accordance with those defined by GEC-ESTRO: 90 Gy_3 for bladder, and 75 Gy_3 for rectum and sigmoid colon.[18, 40]

2.5 Dose calculation and treatment planning

A modified form of the American Association of Physicists in Medicine Task Group 43 (TG-43)[41, 42] technique was applied as the basis for RSBT dose calculation according to:

$$\dot{D}_m(\vec{r}) = S_k \Lambda \frac{G(\vec{r})}{G(\vec{r_0})} g(\vec{r}) F(\vec{r}) T_m(\vec{r}), \tag{5}$$

in which $\dot{D}_m(\vec{r})$ is the dose rate at point $\vec{r}$ with the origin at the center of the eBx point source, where (**Figure 6**):

$$\vec{r} = \vec{r_i} = \vec{v_i} - \vec{h}(\ell), \tag{6}$$

and m is an index standing for the angular course of the shield opening pointed in azimuthal direction $\varphi_m = (m-1)\delta\varphi$, where $m = 1, 2, \dots, 16$, and $m = 1, 2, \dots, 6$, for S-RSBT and H-RSBT, respectively, and $\delta\varphi = 22.5°$ and $\delta\varphi = 60°$ for S-RSBT and H-RSBT, respectively. In the equation above, S_k is the air kerma strength of the eBx source, which is 1.4×10^5 U according to Rivard et al (2006),[43] Λ is the dose rate constant, which is 0.495 cGy U^{-1} h^{-1},[43] $G(\vec{r})$ is the geometry function, $\vec{r_0}$ is a reference point at distance 1

cm lateral from the core of the source, $F(\vec{r})$ is the anisotropy function, and $T_m(\vec{r})$ is the shield transmission function which is defined as:

$$T_m(\vec{r}) = \begin{cases} 1 & \text{if } a^+ = \vec{r} \cdot \hat{a}_P^+ \leq 0 \ \& \ a^- = \vec{r} \cdot \hat{a}_P^- < 0 \ \& \\ & \quad\quad b^+ = \vec{r} \cdot \hat{b}_P^+ \leq 0 \ \& \ b^- = \vec{r} \cdot \hat{b}_P^-, \\ 0 & \text{otherwise}, \end{cases} \tag{7}$$

where $\hat{a}_P^+$, $\hat{a}_P^-$, $\hat{b}_P^+$, and $\hat{b}_P^-$ are, respectively, defined in the $(\hat{x}, \hat{y}, \hat{z})$ coordinate system (**Figure 6** and **Figure 7**) as:

$$\hat{a}_P^+ = \cos[\alpha_m(\ell)]\cos\left(\frac{\Delta\theta_S}{2} + \frac{\pi}{2}\right)\hat{x}(\ell) + \sin[\alpha_m(\ell)]\cos\left(\frac{\Delta\theta_S}{2} + \frac{\pi}{2}\right)\hat{y}(\ell)$$
$$+ \sin\left(\frac{\Delta\theta_S}{2} + \frac{\pi}{2}\right)\hat{z}(\ell), \tag{8}$$

$$\hat{a}_P^- = \cos[\alpha_m(\ell)]\cos\left(\frac{\Delta\theta_S}{2} + \frac{\pi}{2}\right)\hat{x}(\ell) + \sin[\alpha_m(\ell)]\cos\left(\frac{\Delta\theta_S}{2} + \frac{\pi}{2}\right)\hat{y}(\ell) \tag{9}$$
$$- \sin\left(\frac{\Delta\theta_S}{2} + \frac{\pi}{2}\right)\hat{z}(\ell),$$

$$\hat{b}_P^+ = \cos\left[\alpha_m(\ell) + \left(\frac{\Delta\varphi_S}{2} + \frac{\pi}{2}\right)\right]\hat{x}(\ell) + \sin\left[\alpha_m(\ell) + \left(\frac{\Delta\varphi_S}{2} + \frac{\pi}{2}\right)\right]\hat{y}(\ell), \tag{10}$$

$$\hat{b}_P^- = \cos\left[\alpha_m(\ell) - \left(\frac{\Delta\varphi_S}{2} + \frac{\pi}{2}\right)\right]\hat{x}(\ell) + \sin\left[\alpha_m(\ell) + \left(\frac{\Delta\varphi_S}{2} + \frac{\pi}{2}\right)\right]\hat{y}(\ell). \tag{11}$$

As shown by **equation (7)**, $T_m(\vec{r})$ is set to zero when $\vec{r}$ is obscured by the shield and unity otherwise. As the transmission of the 500 micron thick tungsten shield is less than 0.1%, the transmission factor is simply taken to be zero in this study. The radial dose and anisotropy functions for the eBx source were obtained from Rivard et al (2006)[43] as well.

center of voxel i

an arbitrary dwell position

$\vec{v}_i$ $\vec{r}_i$

$\hat{n} = \hat{z}'$

$\Delta\varphi_S$

$\Delta\theta_S$

$\hat{y}$

$\hat{x}$

$\hat{z}$

$\Delta\varphi_S$ = Azimuthal Emission Angle
$\Delta\theta_S$ = Zenith Emission Angle
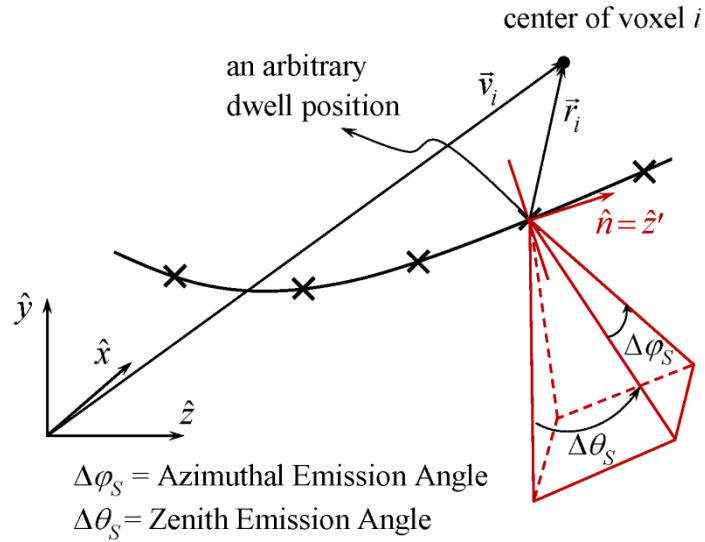
Figure 7: Geometry of a pyramid-shaped beam produced by a cone shield.

In order to ensure a fair comparison between treatment plans of H-RSBT and S-RSBT, the number of RSBT beamlets[44] in H-RSBT is set equal to that in S-RSBT with the assumption that an RSBT beamlet is defined as the dose rate at a point of interest due to a shielded radiation source at a specific dwell position. This uniformity is achieved by decrease of dwell position spacing from 5 mm in S-RSBT to 1.7 mm in H-RSBT and accordingly an increase in the number of H-RSBT dwell positions of over a factor of 2.6. Further, the gradient-based linear least squares method from Shepard et al (2000)[45] was exploited to optimize the dwell times of the dose rate distributions for each beamlet.

2.6 Evaluation

HR-CTV D_{90}, HR-CTV V_{100}, and total treatment time are the metrics used to evaluate all treatment plans for both S-RSBT and H-RSBT techniques. Two azimuthal shield emission angles of 45° and 180° were considered for all patients. According to Dimopoulos et al (2009),[24, 25] in cervical cancer patients treated with the combination of EBRT and BT, the local tumor control probability improves significantly when HR-CTV

22

D_{90} is set to 87 Gy or more. In addition, the HR-CTV V_{100}, the percentage HR-CTV volume receiving a dose of 100 Gy EQD2, was measured as the basis to assess the extent of the HR-CTV hot spots. The total treatment time was also calculated and reported as the total time in which the radiation source positioned inside the patient was irradiating the tumor and did not include the time necessary to reposition the source shield in the keyways when changing emission angles between segments.

3 RESULTS

The EQD2 distributions and corresponding dose volume histograms (DVHs) for all five patients are shown in **Figure 8** and **Figure 9**, respectively. **Figure 10** shows the D_{90} and the treatment time differences of H-RSBT relative to S-RSBT for the two azimuthal emission angles: 45˚ and 180˚. Patients 4 and 5 almost had negligible treatment time differences between H-RSBT and S-RSBT. For patient 3 the D_{90} differences were nearly the same for both 45˚ and 180˚ azimuthal emission angles and were around 1 Gy. H-RSBT in patients 1 and 2 had reduced treatment times relative to S-RSBT for both 45˚ and 180˚ azimuthal emission angles. **Figure 8** shows that the HR-CTV V_{100} values for treatment plans with 45˚ azimuthal emission angle are substantially higher than those with 180˚ azimuthal emission angle in both S-RSBT and H-RSBT.

24
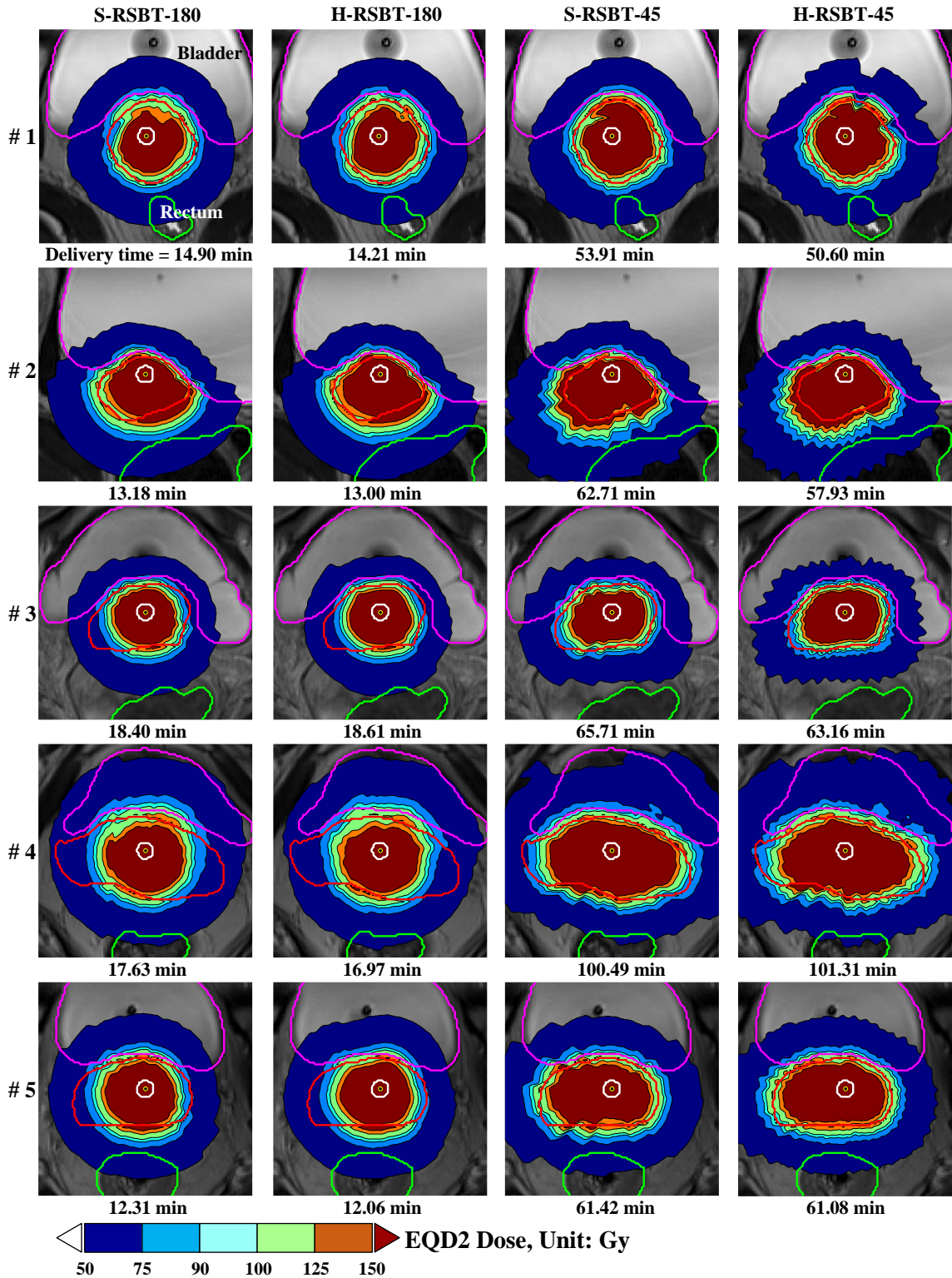
Figure 8: Dose distributions for the cervical cancer patients considered: S-RSBT vs. H-RSBT for both 45˚ and 180˚ azimuthal emission angles.

25
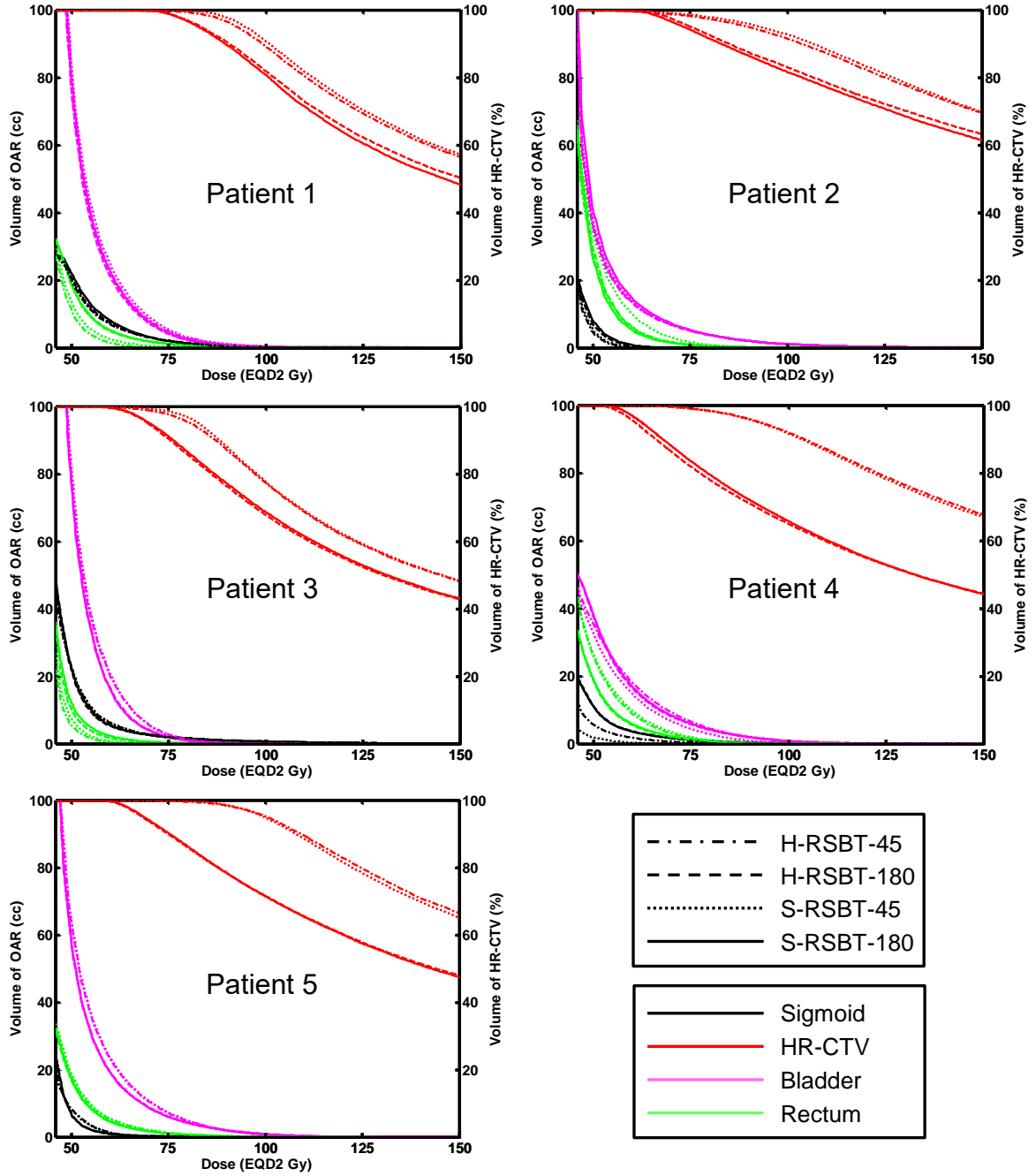
Figure 9: Dose volume histograms for all treatment plannings considered for all five patients: S-RSBT vs. H-RSBT for both 45˚ and 180˚ azimuthal emission angles.
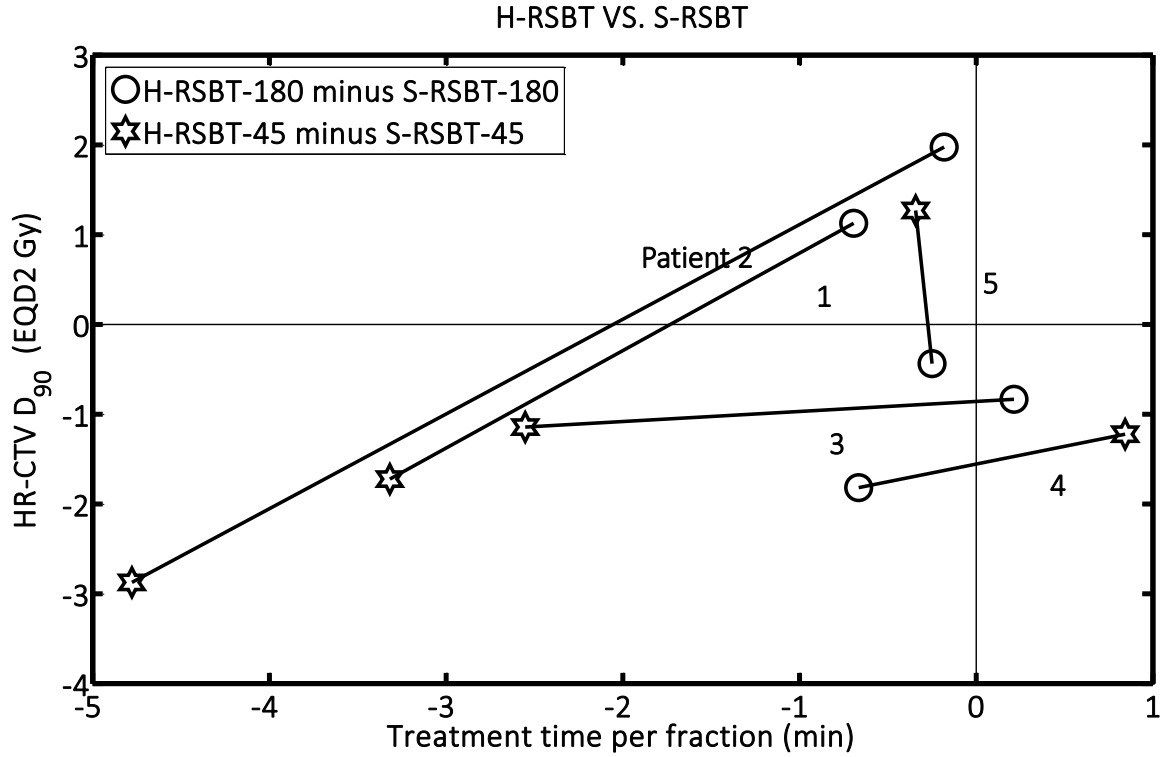
Figure 10: D_{90} and treatment time differences for H-RSBT relative to S-RSBT for both 45˚ and 180˚ azimuthal emission angles.

As shown in **Figure 10** the D_{90} tolerances between H-RSBT and S-RSBT were at most ±2.5%. Also the treatment time differences were approximately in the range of -7% to 1%. The range of delivery times, shown in **Figure 8**, for H-RSBT with the 180˚ and 45˚ azimuthal emission angles was 12.06 to 18.61 minutes and 50.6 to 101.31 minutes, respectively. Thus the 45˚ azimuthal emission angle plans would require over four times as long to deliver as the 180˚ emission angle plans. The average treatment time decrease per fraction of H-RSBT relative to S-RSBT for all patients was 2.8%. The average D_{90} decrease of H-RSBT relative to S-RSBT was clinically irrelevant, at 0.65%.

4 DISCUSSION

4.1 H-RSBT sensitivity analysis

A benefit of H-RSBT is that a shield angle monitoring system is not necessary, as shield angle is parameterized by translational position. There is a drawback to this, however, as uncertainty in shield emission angle is proportional to uncertainty in longitudinal source position. As the longitudinal eBx source position is known to within the standard ±1 mm and the designed shield rotates once every 33.3 mm, then the shield emission angle is only known to within (±1 mm) (360° / 33.3 mm) = ±10.8°. A sensitivity analysis was performed to determine the dosimetric impact of such errors, which is summarized in **Table 3** for the two extreme cases of -1 mm and +1 mm of systematic longitudinal positioning errors. For each patient, only one OAR tolerance dose was violated when a ±1 mm systematic shift occurred. HR-CTV underdose always occurred, and the underdose ranged from 2% to 16%. The observed dosimetric changes resulting from the longitudinal positioning uncertainty represent extreme cases, as positional uncertainty will have both random and systematic components which, combined with fractionation of the deliveries over 5 sessions will have a dose-blurring effect, reducing the overall dosimetric uncertainty. Once a prototype system is developed, the random and systematic source positioning uncertainties can be quantified and a more realistic sensitivity analysis performed. It may also be warranted to develop a robust or worst-case optimization technique for H-RSBT that generates dose distributions that are relatively intensive to the worst-case dwell position errors.

28

Table 3: Effects of systematic longitudinal source positioning errors on dose to the HR-CTV, and OARs for 45˚ azimuthal emission angle. Only the OAR D_{2cc} values for which the D_{2cc} tolerance was violated following the positioning errors were included. OAR tolerance D_{2cc}-values for sigmoid colon, rectum, and bladder were 75 Gy$_3$, 75 Gy$_3$, and 90 Gy$_3$, none of which were violated when there is no positioning error.

Patient	Longitudinal Positioning Error (mm)	HR-CTV D_{90} Change (%)	Sigmoid Colon D_{2cc} (Gy$_3$)	Rectum D_{2cc} (Gy$_3$)	Bladder D_{2cc} (Gy$_3$)
1	-1	-2.15	76.18		
	+1	-2.07			93.26
2	-1	-6.31			97.89
	+1	-6.17			98.24
3	-1	-3.54	75.89		
	+1	-3.4	75.97		
4	-1	-15.67	78.71		
	+1	-5.18			102.24
5	-1	-6		75.62	
	+1	-4.96			105.8

It is expected that H-RSBT deliveries would be based on MR-imaging, which would require the accurate reconstruction of the applicator such that the locations of the helical keyways are well-known for treatment planning and delivery. As the applicator reconstruction would be template-based, a key need will be accurately localizing the applicator tip. Effective quantification of the applicator tip positioning accuracy using MR imaging will not be possible until the applicator is constructed, and enabling sub-millimeter applicator reconstruction accuracy is an important design consideration.

4.2 Treatment planning: H-RSBT vs. S-RSBT

In order to facilitate a straightforward dosimetric comparison, the dose distributions shown in **Figure 8** were generated using HR-CTV dose escalation in which the HR-CTV D_{90} is maximized until the D_{2cc} EQD2 constraint on either of three OARs is

29

reached. In clinical practice, the physician may prefer to compromise OAR sparing in order to avoid underdosing the tumor, or stop the dose escalation once a prescribed HR-CTV D_{90} has been reached, thus delivering OAR doses that are all below tolerance.

H-RSBT and S-RSBT have similar dose conformity, but the treatment time of H-RSBT is approximately 3% less than that of S-RSBT. Further, the DVHs (**Figure 9**) demonstrate that H-RSBT and S-RSBT techniques have D_{90} values within ±2.5% for the HR-CTV and D_{2cc} values within ±3.5% for the three OARs. Dose distributions generated with the 45º azimuthal angle shield are more conformal to the HR-CTV than those generated with the 180º azimuthal shield, but at the expense of a considerable increase in the treatment time of over a factor of four. This fact is directly due to the difference in emission window which controls the amount of energy per unit time at each dwell position. The HR-CTV D_{90}, treatment time, and HR-CTV V_{100} were greater on average for RSBT-45 than RSBT-180 by factors of 1.3, 4.5, and 1.1, respectively. As shown in **Figure 10**, H-RSBT provided a shorter treatment time than S-RSBT for 8 of those 10 treatment plans. However the associated D_{90} values decreased except for 3 treatment plans. In general H- or S-RSBT-45 methods provide HR-CTV D_{90} benefit relative to those plans with 180º azimuthal emission angle.

The HR-CTV V_{100} values were high compared to those values of common ^{192}Ir-based ICBT techniques. This can lead to a uterine overdose. This effect is mainly due to both source specifications and the RSBT treatment time. The dose from the eBx source is proportional to the inverse cube radial distance from the source while that from ^{192}Ir sources is proportional to the inverse square of the radius. Further, the treatment time in RSBT is increased compared to the common ICBT techniques in order to guarantee the

30

tumor coverage. Greater irradiation time is corresponding to a greater dose in the tissues around the source. However the maximum tolerable hot spots in cervical cancer BT are not clear due to lack of clinically relevant data.

In the clinical application of H-RSBT for cervical cancer, one has to employ all the six combinations of keys and keyways engagements (as shown in **Figure 5** and explained at 2.2) in order to make sure of the tumor irradiation coverage. Delivering H-RSBT with an apparatus that enables the retraction and reinsertion of the source/shield in order the shield keys to occupy all of the six combinations of keyways in an automatically changing fashion would accomplish the automation of all of the clinical implementation steps of H-RSBT technique and would improve dosimetric radiation and tumor conformity and also reduce the treatment time. Another advantage of H-RSBT in terms of clinical implementation is its flexibility to adapt to a given patient's cancer stage and shape of the tumor. Based on each patient's cervical cancer stage and the GTV (Gross Tumor Volume) invasion shape, a set of optimal shield with specific zenith and azimuthal emission angles and a set of optimal dwell times need to be employed.

The H-RSBT system has the flexibility in using different shields with different geometrical specifications in a single treatment plan. As there are already six different combinations of keys and keyways and all of them have to be accounted for, different shields can be employed in different combinations. One can use up to six different shields with different azimuthal and zenith emission directions to enhance the D_{90} values and reduce the treatment time provided that a professional optimizer defines the related parameters in advance. However this capability of H-RSBT technique has not been explored yet. Furthermore, in some cases which are of less locally advanced cervical

31

tumor, all of those six keys and keyways combinations might be redundant and those can be reduced to three. This can lead to a decrease in treatment time.

4.3 H-RSBT applicator prototype

The curved helical applicator was produced with an additive manufacturing process through using Polyjet 3D Printing via a 3D printer of Stratasys Objet Eden 350. Polyjet 3D printing utilizes a solid reusable build platform (usually anodized aluminum), a High-resolution multiport liquid resin printer head, and an Ultra Violet (UV) curing lamp array in order to deposit and cure photosensitive polymer resin. The Build Platform, Print Head, and UV lamps are CNC controlled to deposit object profiles in sequential "sliced" vertical layers. A 3D object is produced by stacking and curing these layers of material and support (additively grown vertically). Each layer consists of two types of resin; a material resin and a support resin. The material resin will solidify as the end product; which simulates common plastics such as ABS. The support material will solidify in a manner that supports cantilevered portions of the object being built. Without this support, these cantilevered parts of the 3D printed object would collapse due to gravity during the build process. This support is later removed by manual methods through which a power washing system is utilized to dissolve the support, leaving behind the desired object.

To utilize Polyjet technology, the catheter design was converted to a compatible digital format derived from its original 3D Parametric CAD Model in a process called CAM Programming for Additive manufacturing (Computer Assisted Machine Programming). This process is commonly known as slicing. The initial step is to convert the Parametric CAD model into a format compatible with the slicing program. This

32

universal format is called a Stereolithograph file or .stl file. It is composed of a 3D mathematical approximation of the object utilizing triangles to describe the surface of the object. Generally, the higher the triangle count, the better the resolution of the translated representation and the more compatible to the accuracy of the original design.

In the second step of CAM, the .stl file is then sliced in the slicer software. In this case Stratasys employs a proprietary slicer software called Objet Studio. Objet Studio sections the .stl file vertically into slices. Each slice digitally represents the boundary profile of the object at specific heights. This boundary profile is then used to write a toolpath by which the printer head will travel and deposit resins. Objet Studio must specify the outer boundary, the interior fill pattern, the differential between material, the support resin deposits, and the UV lamp cure time for each individual layer. Objet Studio then compiles these toolpaths into a single toolpath file for each object. It also dictates the number of parts to produce and the orientation of those parts on the build platform. In the final stage, Objet Studio translates the combined toolpaths for all objects into machine coordinates and also into the codes that the printer can translate them into the specific set of motions. This final Stratasys proprietary file type is .obj.

Figure 11: H-RSBT applicator prototype.

Once the 3D print is completed, the object (encased in support) is moved to a power washing station and the support is removed using high pressure water jets. The result is the curved applicator with interior helical channels as shown in **Figure 11**.

4.4 Conclusion

H-RSBT is a mechanically feasible technique in the curved applicators needed for cervical cancer brachytherapy. S-RSBT and H-RSBT dose distributions were clinically equivalent for all patients considered, with the H-RSBT deliveries tending to be faster.

Part II. MULTI-SOURCE ROTATING SHIELD BRACHYTHERAPY APPARATUS FOR PROSTATE CANCER[2]

---

[2] Most of the content of this part is accepted for publication in International Journal of Radiation Oncology, Biology, Physics under the title of "Multisource Rotating Shield Brachytherapy Apparatus for Prostate Cancer."

5 INTRODUCTION

5.1 Prostate cancer brachytherapy and complications

Prostate Cancer is the third leading cause of male cancer mortality in developed countries[46] and the most prevalent non-cutaneous cancer in men, with 220,800 new diagnoses in 2015 in the U.S.[47] and more than one million new cases, each year, throughout the world.[1] Beyond 3 million men in the U.S. are estimated to suffer from prostate cancer[48] which is mostly diagnosed as a clinically localized cancer.[49] Although long-term (10+year) biochemical disease-free survival is high and tends to increase in recent years, more than 27,500 men in the U.S. are estimated to have died of prostate cancer in 2015.[47] Generally, men have a chance of one in six of developing prostate cancer during their lifetime.[50]

Management methods are controversial[51] and a variety of treatment options including radical retropubic prostatectomy,[52, 53] EBRT monotherapy,[54-56] low-dose-rate (LDR) monotherapy,[57-59] HDR-BT monotherapy,[60-70] and EBRT in combination with LDR, pulsed-dose-rate, or HDR brachytherapy[71-80] are offered thereof. Treatment of intermediate- or high-risk prostate cancer with EBRT followed by HDR-BT boost has been shown to be superior to EBRT or BT alone, particularly in terms of treatment efficacy, the reduction in the risk of recurrence, and the improvement in biochemical control.[79, 81-83] However, as recent advances in radiotherapy techniques added variety to prostate cancer treatments, one must be armed with the knowledge of short- and long-term health related outcome of each modality.[84] While achieving tumor control is paramount, prostate cancer patients may live with the side effects of their treatment for decades, and anticipated side effects play a strong role in treatment decisions.[85, 86]

Urinary incontinence/stricture, urinary irritation/obstruction, erectile dysfunction, and bowel toxicity are long-term postoperative adverse effects associated with such treatment modalitiies.[87-92] Patients treated with EBRT and/or BT are more prone to post-therapeutic bowel complications and short-term urinary obstruction/irritation than those treated with surgery alone. However, radiation therapy techniques are less invasive than radical prostatectomy, concerning postoperative genitourinary complications.[85, 93] Urinary retention (ischuria) and urethral stricture experienced by patients undergoing BT monotherapy or EBRT with HDR-BT boost were statistically significant compared to that experienced by patients undergoing EBRT alone.[91, 94] In addition, acute bowel/rectal toxicity rate in patients treated with combined EBRT and HDR-BT was greater than the same complication rate in patients treated with HDR-BT monotherapy.[91] Urethral stricture, occurring mostly in bulbomembranous urethra or apex/external sphincter region,[95] is the most frequent nontrivial late toxicity of combined EBRT and HDR-BT treatments.[96] The associated reported rates (5.2%,[84] 6.6%,[97] 8%,[96] and 10%[91]) are considerably greater than those reported for EBRT monotherapy (1.7%,[84] 2%,[91] and 3%[98, 99]). Urethral brachytherapy dose is most probably the underlying cause of urethral stricture in combined EBRT and HDR-BT treatments.[100-103] The posterior radiation-induced urethral stricture is generally difficult to manage and the limited treatment options that performed are often accompanied by urinary incontinence.[104-106]

Existing brachytherapy techniques offer advantages over other treatments in both survival and side effects with the exception of increased urinary complications. In a large scale literature review, Grimm et al. (2012)[107] found that in low-risk patients brachytherapy provides superior long-term (10+ year) biochemical relapse-free survival

to EBRT and surgery, in intermediate-risk patients brachytherapy alone is equivalent to EBRT in combination with brachytherapy and superior to surgery and EBRT alone, and in high-risk patients EBRT in combination with brachytherapy is superior to more localized treatments such as surgery alone, brachytherapy alone, or EBRT alone. The benefits of brachytherapy in obtaining long-term relapse-free survival are suspected to be due to the dose escalation achievable that would not be possible with EBRT alone.[108] Surgery, even using the Da Vinci robot (Intuitive Surgical, Inc., Sunnyvale, CA),[109] has been reported to have greater risks of urinary incontinence and sexual dysfunction than radiotherapy techniques,[110] in that brachytherapy has a 3-fold higher rate of return to baseline urinary function compared to surgery at 36 months, and it has a 5-fold higher rate of return to baseline sexual function.[110]

5.2 RSBT as an alternative to HDR-BT for prostate cancer

OARs (urethra, rectum, and bladder)[80] inside and adjacent to the clinical target volume (CTV)[80] (**Figure 12**)[111] adversely affect the deliverable HDR-BT dose to the prostate. Hence, the target conformity and attainable dose escalation as well as the healthy organ sparing capability of conventional interstitial HDR-BT dose distributions are restricted based on the geometrical constraints imposed by the position and shape of the catheters, as well as the radially symmetric radiation dose distributions emitted by conventional unshielded BT sources. Dose distribution conformity and sensitive healthy tissue avoidance can be considerably improved through the use of rotating shield brachytherapy (RSBT) in conjunction with a specific radiation source amenable to shielding. The notion of RSBT was first conceived by Ebert,[112, 113] and studies on developing clinically plausible RSBT delivery techniques were performed for rectal,[31, 114]

breast,[115] cervical,[32, 34, 35] and prostate cancer.[116] With RSBT, radiation sources are partially shielded and have the freedom to rotate in an optimized fashion[33, 44] such that radiation dose is directed away from sensitive structures and into the targeted tissue. However, the conventional prostate cancer HDR-BT radioactive sources, such as ^{192}Ir and ^{60}Co,[117] are not suitable for shielding in very limited space of a 14-gauge catheter used in interstitial BT of prostate cancer. An alternative radioisotope of ^{153}Gd is recently proposed[118] as an intermediate radioactive source, which is capable of being shielded with an only 600 µm thick platinum cap, and its application in constructing an RSBT shielded catheter for prostate cancer treatment is also investigated.[116]
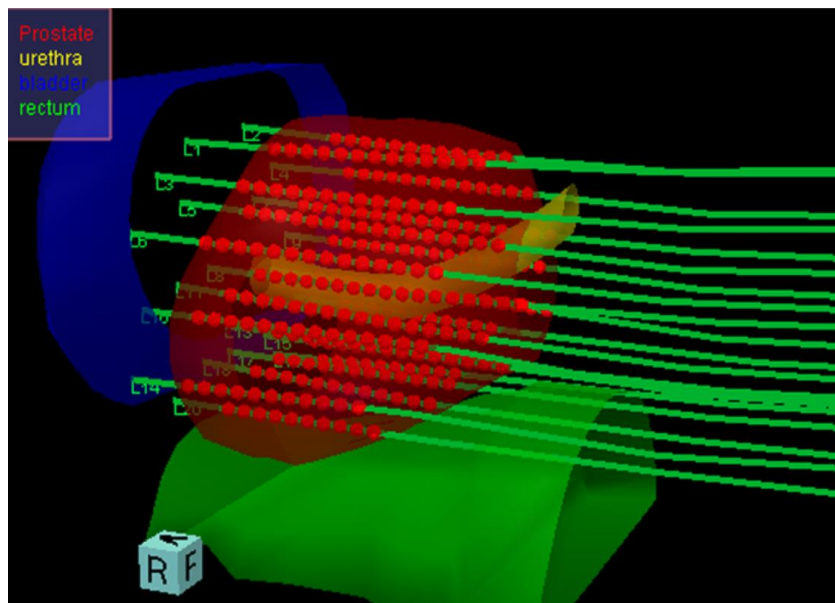
Figure 12: 3-D reconstruction of the CTV and OARs in HDR-BT of prostate cancer.

Existing prostate cancer treatments often cause significant long-term side effects. RSBT employs novel technology to provide optimal cancer control while reducing side effects. **Figure 13** shows the differences between conventional HDR-BT (top row) and RSBT (bottom row) for a prostate cancer clinical case. The innovation of RSBT is that a novel radiation source, ^{153}Gd (242 day half-life, 60.9 keV average photon energy), is used

39

instead of conventional ^{192}Ir (74 day half-life, 360 keV average energy), combined with partial shielding of the source. Partial source shielding (**Figure 13b**) enables a deliberately non-symmetric dose distribution (**Figure 13d**) about an implanted needle.[116] Each of the 15–20 nitinol needles contains a catheter that is slowly and incrementally rotated throughout treatment to deliver the desired dose distribution. The dwell times within each catheter are modulated so that radiation is emitted for a longer time in some directions (into tumor) than others (into urethra/rectum/bladder), without compromising tumor dose (**Figure 13e–h**). The RSBT approach overcomes the rectum, bladder, and urethra dose limitations of conventional HDR-BT, which constrain prostate dose.

The central prostate cancer RSBT clinical procedures would be the same as conventional HDR-BT in that the sterilizable needles will be implanted under trans-rectal ultrasound (US) guidance while the patient is under anesthesia, a radiation treatment plan is generated based on the imaged needle positions, and the treatment is delivered. However after image acquisition the removal of the US probe is done as a method of keeping the anterior rectal wall away from the posterior prostate (i.e., the radiation sources).[119]

An economically-viable radiation source with an appropriate photon energy spectrum for interstitial shielding other than ^{153}Gd is not available currently.[118] As ^{153}Gd has a lower dose rate than ^{192}Ir, RSBT delivery takes longer than the 30 minutes or less required for HDR-BT. Our proposed RSBT system employs simultaneously controlled 62 GBq (1.5 Ci) ^{153}Gd sources, enabling the delivery of a 10 Gy dose in an about 60 minutes. The increased procedure times would be clinically acceptable primarily due to the clinical advantages RSBT can provide.

40

Clinical Source/Needle/Catheter Attributes

Cross Section

Dose Distribution In Axial Plane

Conventional High-Dose-Rate Brachytherapy

a.

c.

Rotating Shield Brachytherapy

b.

d.
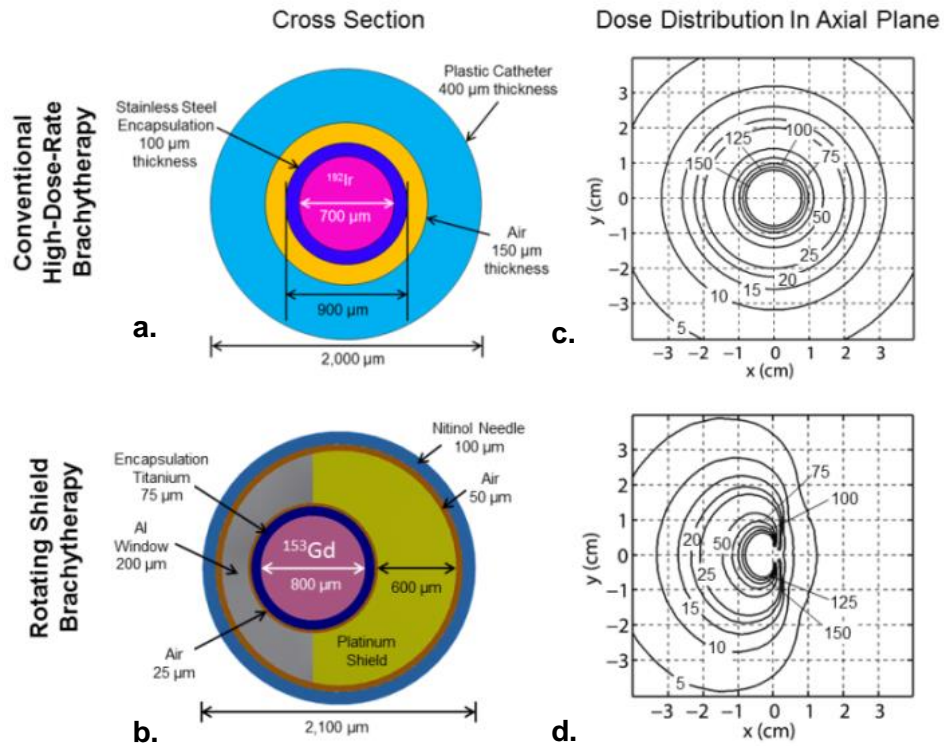
Prostate Dose Distributions

0 mm Urethral Margin

3 mm Urethral Margin

Dose (%)

e.

g.

f.

h.
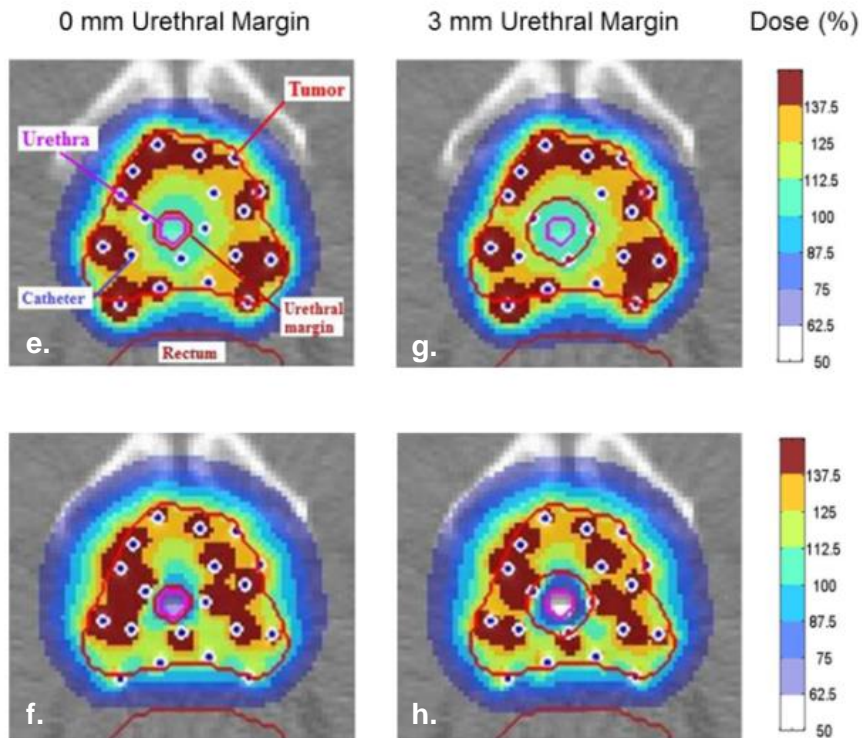
Figure 13: Differences between conventional HDR-BT (top row) and ^{153}Gd-based RSBT (bottom row). **(a)** Where a radially symmetric needle/source system is used for HDR-BT, **(b)** a needle/source system with a spatially-offset ^{153}Gd source and a high-atomic number (e.g., platinum) shield would be used for RSBT. The dose rate distributions from the sources, normalized to 100% at 1 cm off-axis, are radially symmetric for **(c)** HDR-BT and **(d)** directionally biased for RSBT. The resulting dose distributions have reduced doses to the urethra, rectum, and bladder, when the minimum dose delivered to the hottest 90% (D_{90}) of the tumor is held constant. For **(e–f)** 0 mm and **(g–h)** 3 mm urethral margins, RSBT reduced the minimum dose to the hottest 0.1 cm^3 of the urethra ($D_{0.1cc}$) by 29% and 38%, respectively. RSBT rectum and bladder D_{1cc}-values (complication predictors) were lower than HDR-BT by 5–7%.

5.3 Objectives of the PhD project

The aim of the current work is to introduce a novel multisource RSBT apparatus, a mechanically feasible RSBT delivery technique for conformal HDR-BT of prostate cancer. The innovative interstitial RSBT (I-RSBT) system presented in former study[116] was demonstrated to be capable of lowering the urethral dose up to 44% relative to conventional HDR-BT. However, the authors specified the need for a robust approach in order to deliver therapeutically relevant doses of I-RSBT to prostate. Multisource RSBT apparatus overcomes the technical and clinical barriers to implementation of the previously proposed approach of ^{153}Gd-based I-RSBT for prostate cancer, enabling the delivery of deliberately urethra-sparing dose distributions with higher prostate dose. Clinical implementation of I-RSBT with this novel system provides significant prostate cancer dosimetric improvements relative to conventional interstitial HDR-BT techniques

42

and enables minimizing urethral side effects, urethral stricture in particular, which are difficult to manage, if not impossible.

We proposed multi-catheter RSBT approach as a novel prostate cancer RSBT delivery mechanism and technique through which the rotation and translation of nitinol catheter-mounted source/shields for all implanted needles are controlled simultaneously. Following needle implantation through a patient template by the physician, the delivery system is docked to the patient template. To keep delivery as simple as possible, all of the catheters are held at the same rotation angle at a given time, and the catheters are rotated by translating a moving needle template between two stationary templates (mechanism described in the following sections). The catheters are rotated by 22.5° every 3–4 minutes, and only a single 360° rotation is needed for a full treatment. For each rotation angle, source depth in each needle is controlled by a multi-source afterloader, which is an array of commercially available belt-driven linear actuators to which the source wires will be mounted. The shielded source for each needle can be retracted back into the afterloader within less than 10 seconds in the event of an emergency.

6 METHOD

6.1 Brachytherapy source

Enabling the multisource RSBT technique requires an appropriate radioisotope and a technically feasible rotating shield system that fits inside a 14-gauge needle used for prostate cancer brachytherapy. For this apparatus ^{153}Gd is selected as the source isotope due to its reasonable dose rate, energy spectrum ranging from 40 keV to 105 keV (60.9 keV average), half-life of 242 days, and its potential for mass production via neutron irradiation of ^{151}Eu or ^{152}Gd.[116] A nitinol (NiTi) RSBT needle containing a rotating catheter as well as a shielded ^{153}Gd source was designed, and the dose rate distribution about the partially shielded source was calculated using the MCNP5 Monte Carlo code and a published ^{153}Gd spectrum.[118] ^{153}Gd, with an expected maximum achievable specific activity of 1,850 GBq of ^{153}Gd per gram of Gd, emits photons in the intermediate range of 40-105 keV. The modeled source was a 7.41 g/cm^3 Gd$_2$O$_3$ pellet containing 2,442 GBq of ^{153}Gd per gram of Gd$_2$O$_3$, which could be generated by neutron irradiation of spent dual-photon absorptiometry sources containing about 87% ^{152}Gd. The Monte Carlo dose calculation method is the same as that employed by Adams et al.[116]

The shielded ^{153}Gd source and its calculated relative dose rate distribution are shown in **Figure 14(a)** and **Figure 14(b)**, respectively. The source exhibits azimuthal anisotropy in its dose rate distribution due to the presence of platinum shielding on one side. In the proximal and distal directions, the platinum shield shown in **Figure 14(a)** has cylindrical platinum end cap welded to it that prevent the ^{153}Gd source pellet from sliding out. The end caps function as receivers for the aluminum window, and, when they are welded to the platinum shield, the aluminum window is fixed in place. The dose rate on the platinum shielded side of the source at 1 cm off-axis was to about 7% of that on the

unshielded side. The calculated dose rate of the RSBT source 1 cm from the geometric center of the catheter on the side with the aluminum window and along the axial plane passing through the geometric center of the active radiation source was 6.82×10^2 cGy h^{-1}. The dose rate at 1 cm from the central axis of the ^{192}Ir source was 4.246×10^4 cGy h^{-1} along the axial plane passing through the geometric center of the active source.
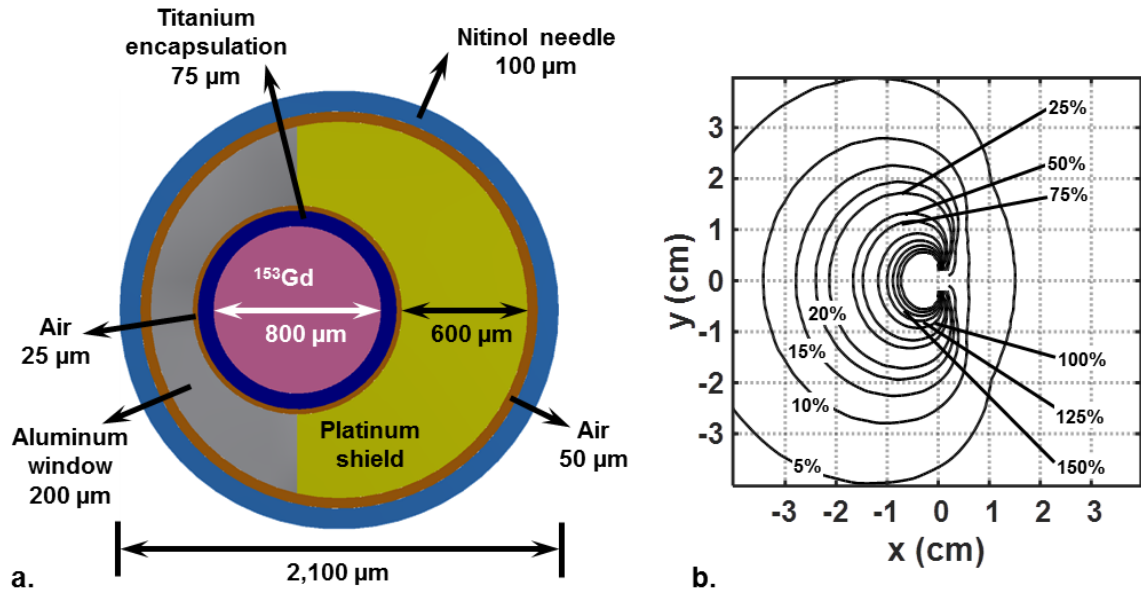
Figure 14: (a) Needle/source system with a spatially-offset ^{153}Gd source and a platinum shield used as the radiation source in multisource RSBT apparatus. **(b)** Directionally biased dose rate distribution from the source/shield, normalized to 100% at 1 cm from the source, shown in a plane perpendicular to the source axis.

6.2 Multisource angular drive mechanism

The RSBT system is equipped with an angular drive mechanism that controls the rotation of nitinol catheter-mounted source/shields for all implanted needles simultaneously. Following needle implantation, the angular drive mechanism is docked to the patient template in which the needles are all held at the same rotation angle at a given time while the catheters are rotated by translating a moving template between two

45

stationary templates using redundant motors. A two-frame conceptual diagram of the angular drive mechanism is shown in **Figure 15**. It consists of the cross section of five points along a single inserted needle starting from the combination of the afterloader wire and the connector to the combination of needle/source/shield inside the prostate. **Figure 15** shows how translational motion of the moving template causes a 180° rotation of a shielded source inside a needle. When the moving template is translated longitudinally the shafts rotate, as threaded holes of the moving template exert enough resistive force to the threaded exterior peripheral wall of the shaft which is fixed axially. The angular orientation of the shielded source is also fixed and known during treatment via a proximal keyed cuff that attaches the remote afterloader wire to the source catheter. Partial shields around the sources are oriented at a known angle by means of the keys and the keyways machined into various parts.

Figure 16 shows the whole multichannel angular drive mechanism with all the shafts and templates, which is docked to twenty inserted needles. As shown, the connector can move freely in the longitudinal direction in order to connect with needles that protrude from the patient at varying distances. The rotating shafts are threaded to provide a pitch with 10 cm translation per shaft rotation (1 mm per 3.6° rotation), which is sufficient to balance the tradeoffs between rotational accuracy, apparatus length, and resistive force exerted on the moving template by the shafts during motion. In order to create the desired translation of the moving template, four motors are arranged to rotate the lead screws contacting the moving template. When the lead screws rotate, the moving template translates longitudinally while the other two templates provide rigidity to the system.
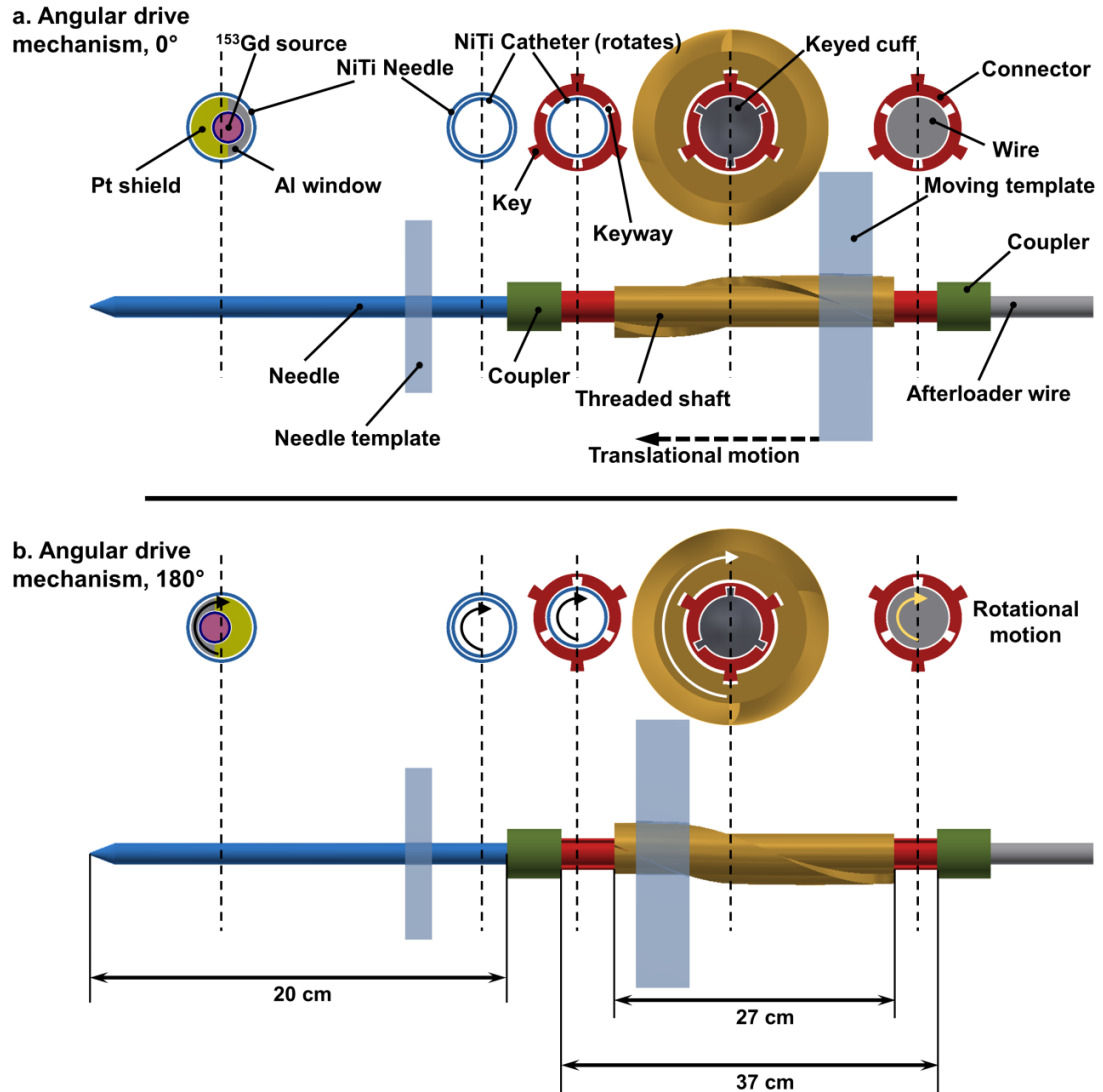
Figure 15: Angular drive mechanism incorporating side views and cross sections of several points along the axis of a single needle. Translational motion of the moving template rotates the shaft, connector, and source/shield/catheter from **(a)** 0° to **(b)** 180° angular positions. Each needle, implanted through the patient template, is coupled to the catheter-mounted afterloader wire through a keyed connector (red), which passes through a rotating shaft. The catheter is rigidly attached to a proximal keyed cuff that enables the angular orientation of the shielded source to be fixed and known at all times during treatment. Items in the figure are not to scale.

47
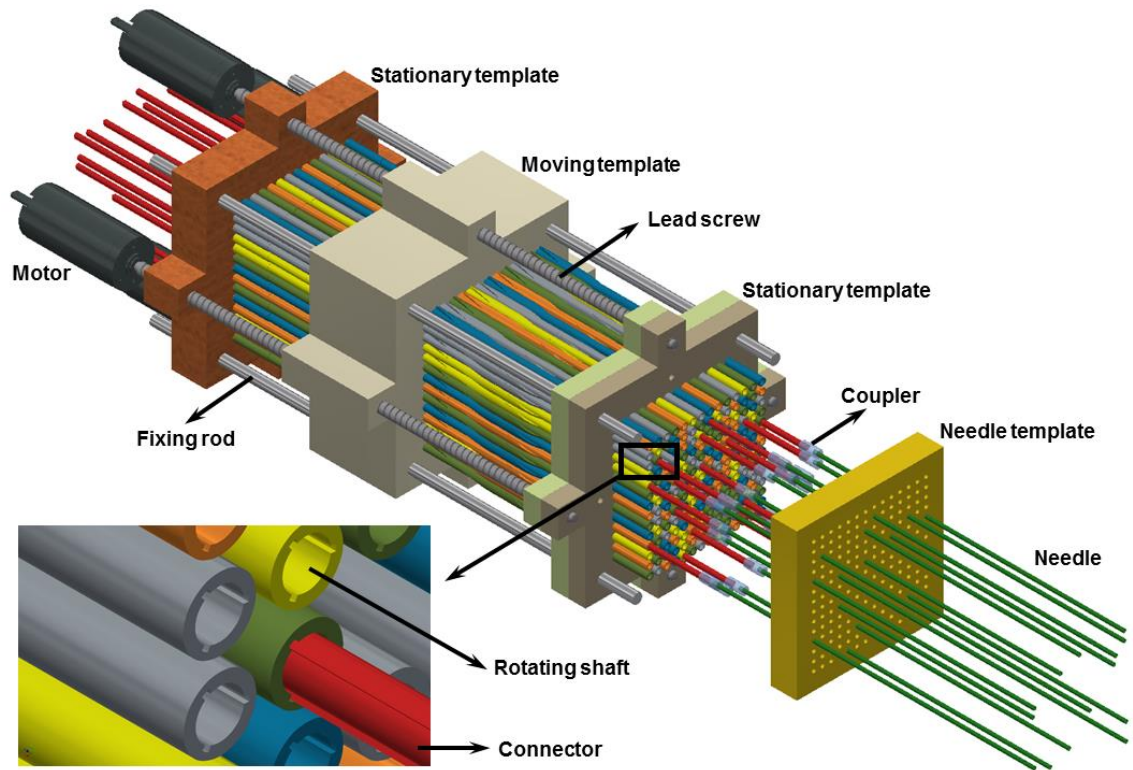
Figure 16: Multichannel angular drive system. All shafts are locked at the same angular orientation at a given time by the moving template, which, when translated, simultaneously rotates all of the shafts. The moving template is translated by redundant motors that are attached to lead screws, and the shaft angular positions are known based on the position of the template. A subset of the connectors (red) is shown in this figure.

6.3 Multisource remote afterloader

The depth positions of the radiation sources are determined via a remote afterloader (**Figure 17**) consisting of twenty Parker-Hannifin® (PH) (Parker, Rohnert Park, CA, USA) 1,000-mm travel belt-driven linear actuators that have 0.2 mm positional reproducibility and are assembled in the vertical orientation. A 1.8-mm-diameter 7×7 flexible stainless steel braided wire is attached to the carriage (yellow) of each actuator and moved back and forth into a guide box through a rigid guide tube and a flexible

adaptive tube, connected to each other. The wire is rigidly attached to a flexible nitinol catheter by means of keyed cuff. The angular orientation of the shielded source, which is attached to the other side of the nitinol catheter, is fixed and known for every dwell position inside each needle, through the engagement of proximal keyed cuffs and the keyways cut into the connector. The overall multisource RSBT system enables controlling the depth positioning as well as the rotations of the shielded sources in a decoupled manner.

49
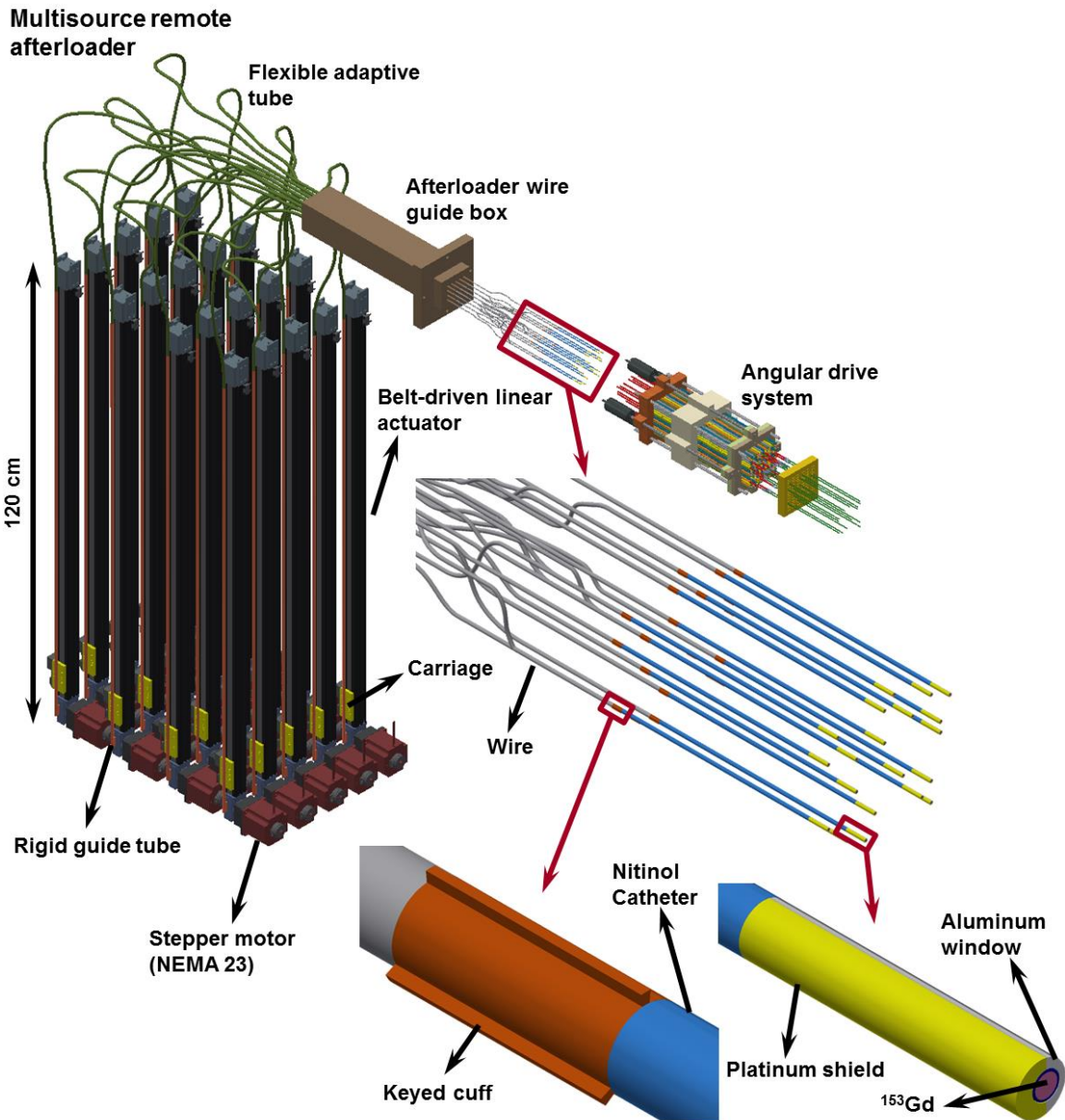
Figure 17: Multisource remote afterloader, consisting of four stacks of five linear actuators in the vertical orientation. A flexible stainless steel braided wire from each actuator is attached to the nitinol catheter (blue) via a keyed cuff and is fed into a guide box. Each shielded source is attached to a nitinol catheter which travels and rotates inside its corresponding needle. The braided wires attached to the linear actuators' carriage require guide tubes as well.

6.4 Dose delivery methodology

A "moving tessellation" approach is proposed in order to maximize the diameter of the shafts under the constraint that the spacing between shaft centers is 5 mm, as shown in **Figure 18**. Based on the spatial tessellation theory,[120] one type or more than one type of shapes can be geometrically designed such that if they are stacked on top and besides each other no space in between the different shapes remains unused. With this design approach, the emission direction for all sources is constant at a given point in time during treatment.
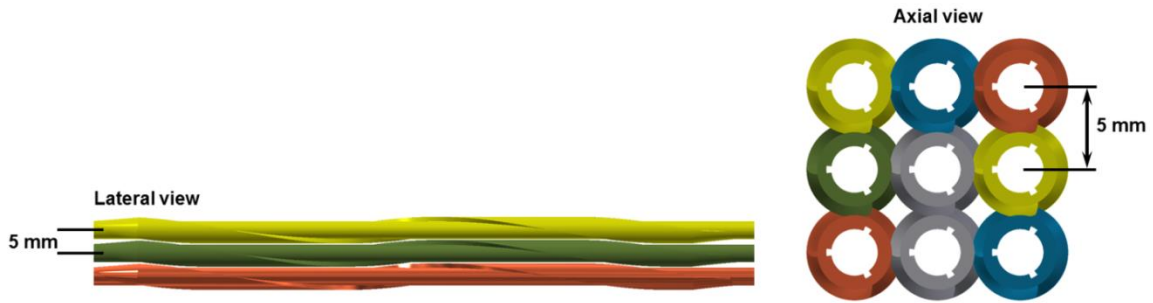
Figure 18: Configuration of a 3×3 shaft array (sampled from 13×13) with a constant center-to-center spacing of 5 mm. Shafts can all rotate simultaneously with no interference.

The delivery process occurs by having the moving template control the angular directions of all the source/shield combinations and using the remote afterloader independently to control the longitudinal position of all the sources in all the needles simultaneously. Once the source angles are changed by translating the moving template, the multisource afterloader moves the sources to all of the necessary depths in each needle. The process is repeated for all of the source rotation angles, and, if one were to use 16 different dwell positions with 16 different shield directions, all of the CTV would be covered while the urethra is spared. Thus, in this technique the catheters are rotated by

51

22.5°, and only a single 360° catheter rotation is needed for a full treatment. The designed angular drive apparatus forces the sources to be at the same angle at the same time while the longitudinal depth of the sources inside needles can be adjusted in different positions. Therefore the total amount of time spent on a specific emission direction is dictated by the catheter that requires the greatest total dwell time to deliver.

The shielded source for each needle can also be retracted back into the afterloader within less than 10 seconds in the event of an emergency. The dose rate of the [153]Gd sources (62.4 GBq) is such that each implanted needle has its own partially-shielded RSBT source while the radiation from all sources can be delivered simultaneously. RSBT delivery with this novel multisource apparatus involves inserting the needles, without catheters, through the perineum under ultrasound guidance. The needles will be CT/MRI compatible, and sterilizable.

6.5 Treatment planning

In order to assess the dosimetric effectiveness, delivery times, and robustness to uncertainties of the proposed RSBT approach, comparative treatment plans for RSBT and HDR-BT were generated on computed tomography (CT) images of a previously treated anonymous patient with an average CTV of 60 cm^3, for whom 19 needles were used. The adjacent dwell positions are all separated by 5 mm and for each dwell position 16 evenly distributed emission directions were created for RSBT delivery. A step and shoot dose delivery model was implemented for all the simulations, in which the source shoots the radiation for a specified and optimized amount of time in each beamlet. Based on the methods of the California Endocurietherapy Institute for treatment planning,[121] a 5-mm margin is added to the prostate boundary, excluding the regions adjacent to the bladder,

52

rectum, and the proximal seminal vesicles, in order to contour the CTV. The urethral margins of 1, 3, and 5 mm were included in the model as a relaxed prescription dose constraint in order to provide a spatial location for the dose gradient about the urethra. The main goal of performing RSBT for patients with locally advanced prostate cancer is enabling substantial urethral sparing relative to conventional HDR-BT. By defining the mentioned urethal dose gradient volumes (1, 3, and 5 mm) around the urethra and including that into the treatment planning system, the urethra is expected to receive a dose much less than that of the conventional HDR-BT, if the physician let that volume receives a dose lower than the prescribed dose. For each margin a specific treatment plan is generated and evaluated. The CTV D_{90} (minimum dose to the hottest 90% of the CTV) is set to 110% of the prescribed dose (20 Gy). CTV V_{100} and V_{150} is required to be in the range of 90% to 100% and <35%, respectively. $D_{0.1cc}$ values for the rectal wall, the bladder wall, and the urethra were limited to less than 85%, 100%, and 110%, respectively. D_{1cc} values for the same set of organs at risk were also limited to less than 80%, 90%, and 105%, respectively.

6.6 Treatment planning optimization

An in-house optimizer is used in order to generate $\vec{t}$, the vector of dwell times in each dwell position and emission direction for every inserted catheter. The optimizer is based on the linear least square method, described by Shepard et al (2000).[45] The optimization method is used for both RSBT and conventional HDR-BT treatment plans.

A quadratic objective function, described in **equation (12)**, is minimized:

$$E(\vec{t}) = \sum_{k=1}^{K} \frac{1}{T_k} \sum_{i \in \tau_k} \left[\beta_k^+ H^2(d_i - d_k^+) + \beta_k^- H^2(d_k^- - d_i) + \beta_k^{V+} C_{(0, \Delta D_k^{V+})}^2 (d_i - d_k^{V+}) \right] \qquad (12)$$

53

$$s.t. \ t_j \geq 0,$$

where:

$$H(x) = \begin{cases} x & x \geq 0 \\ 0 & otherwise, \end{cases} \tag{13}$$

and

$$C_{(a,b)}(x) = \begin{cases} x & a \leq x \leq b \\ 0 & otherwise, \end{cases} \tag{14}$$

and

$$d_i = \sum_j D_{ij} t_j, \tag{15}$$

in which d_i is the cumulative dose at voxel i, and D_{ij} is the dose rate at voxel i and beamlet j, with the optimization parameters defined in **Table 4** and specified by their values in **Table 5**.

Table 4: Definitions of optimization parameters.

Parameter	Definition
τ_k	Subset of voxel indices that are inside tissue k.
T_k	Number of voxels that are inside tissue k.
$d_k^{\pm}$	Dose threshold for overdose (+) and underdose (−), for tissue k.
$\beta_k^{\pm}$	Penalty weight for overdose (+) and underdose (−), for tissue k.
d_k^{V+}	Dose threshold for dose-volume overdose (+) for tissue k.
V_k^{+}	Percent volume threshold for dose-volume overdose (+) for tissue k.
β_k^{V+}	Penalty weight for dose-volume overdose (+) for tissue k.
ΔD_k^{V+}	Difference between the dose planned and desired to V_k^{+} in the cumulative dose-volume histogram for tissue k.

Table 5: Optimization parameter values for RSBT and HDR-BT treatment plans. NT is normal tissue. N/A means not applicable.

Tissue	β_k^+	d_k^+	β_k^-	d_k^-	β_k^{V+}	d_k^{V+}	V_k^+
CTV	0	N/A	1000	120%	0	N/A	N/A
Urethra	50	50%	0	N/A	0	N/A	N/A
Bladder	5	50%	0	N/A	20	50%	1%
Rectum	20	20%	0	N/A	20	50%	1%
NT	2	80%	0	N/A	0	N/A	N/A

6.7 Uncertainty tolerance

A sensitivity analysis based on an extensive treatment planning study was performed in order to estimate the dosimetric impact of uncertainty in both longitudinal position and emission angle of the shielded catheters. A combination of multiple different systematic longitudinal positioning errors (≤ 2 mm) as well as rotational orientation errors ($\leq 15°$) of the shielded catheters is considered in order to determine the uncertainty tolerance of the RSBT multisource delivery system. As applying positional and rotational errors affects directly on DVH parameters, CTV D_{90} and urethra $D_{0.1cc}$ were evaluated to quantify plan degradation due to uncertainty. Deviation of those two parameters from the baseline shows how much uncertainty can be tolerable in order to deliver a dose with $\pm 3\%$ accuracy for CTV $D_{90\%}$ and urethra $D_{0.1cc}$. The assumption is based on the plausible scenario of rotating all of the catheters the same incorrect angle as well as translating all of the catheters the same incorrect distance.

7 RESULTS

7.1 Multisource ^{153}Gd-based RSBT vs. conventional HDR-BT with ^{192}Ir

Table 6 shows a comparison between the dosimetric parameters of conventional HDR-BT with ^{192}Ir and the ^{153}Gd-based multisource RSBT, along with the volume associated with each tissue of interest. Planned conventional HDR-BT and ^{153}Gd-based multisource RSBT dose distributions are displayed and compared in **Figure 19**, **Figure 21**, **Figure 23**, and **Figure 25** for the urethral gradient margins of 0, 1, 3, and 5 mm, respectively. **Figure 20**, **Figure 22**, **Figure 24**, and **Figure 26** shows the corresponding overlaid DVHs.

Table 6: Dose values of target and organs at risk for ^{153}Gd-based I-RSBT with multisource apparatus compared to a common HDR-BT with ^{192}Ir. P-Urethra is the peri-apical urethra. D_m is mean dose in the tissue. N/A means not applicable. A 3-mm ring is defined surrounding the urethra in both techniques.

Tissue	Volume (cc)	BT technique	D_m (Gy)	D_{90} (Gy)	V_{100Gy} (%)	V_{150Gy} (%)	D_{1cc} (Gy)	$D_{0.1cc}$ (Gy)
CTV	32.36	HDR-BT with ^{192}Ir	139.6	109.18	97.96	20.81	N/A	N/A
		RSBT with ^{153}Gd	140.7	109.22	95.8	29.28	N/A	N/A
Urethra	1.48	HDR-BT with ^{192}Ir	92.5	N/A	N/A	N/A	92.49	103
		RSBT with ^{153}Gd	64.6	N/A	N/A	N/A	65.23	71.4
P-Urethra	0.35	HDR-BT with ^{192}Ir	75.2	N/A	N/A	N/A	N/A	89.69
		RSBT with ^{153}Gd	60.7	N/A	N/A	N/A	N/A	67.4
Bladder	110.4	HDR-BT with ^{192}Ir	16.99	N/A	N/A	N/A	58.99	73.54
		RSBT with ^{153}Gd	20.36	N/A	N/A	N/A	60.68	81.82
Rectum	89.87	HDR-BT with ^{192}Ir	19.7	N/A	N/A	N/A	60.61	72.03
		RSBT with ^{153}Gd	23.6	N/A	N/A	N/A	65.65	80.41

56

Figure 19: Dose distribution for 0-mm urethral margin of (a) [192]Ir based HDR-BT and (b) [153]Gd based I-RSBT with multisource RSBT apparatus sampled onto a CT scan of a prostate cancer patient.
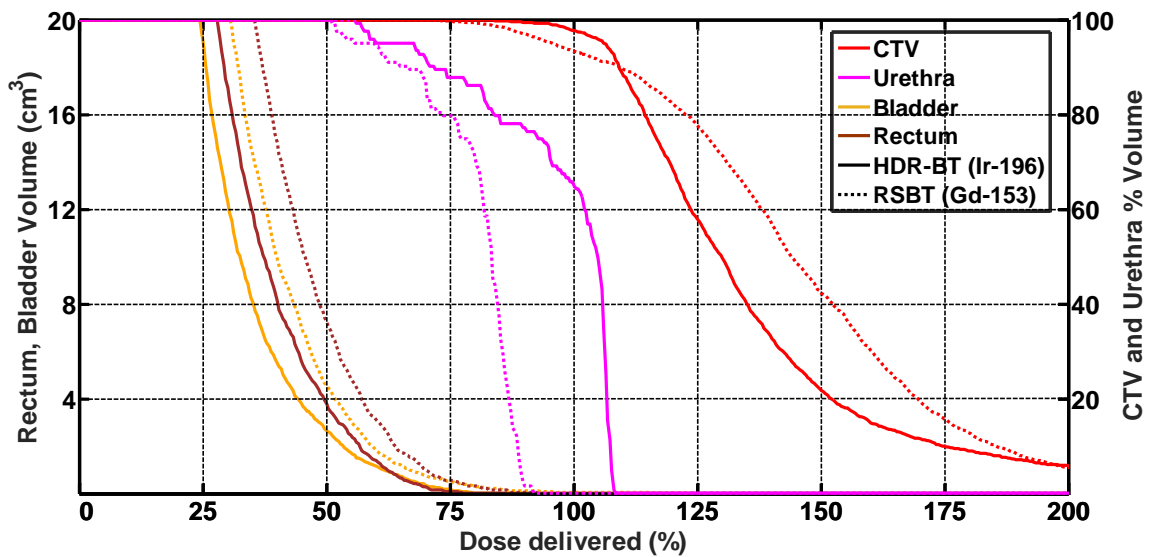
Figure 20: Dose-volume histograms for conventional ^{192}Ir based HDR-BT and [153]Gd based I-RSBT with multisource RSBT apparatus for urethral margin of 0 mm.
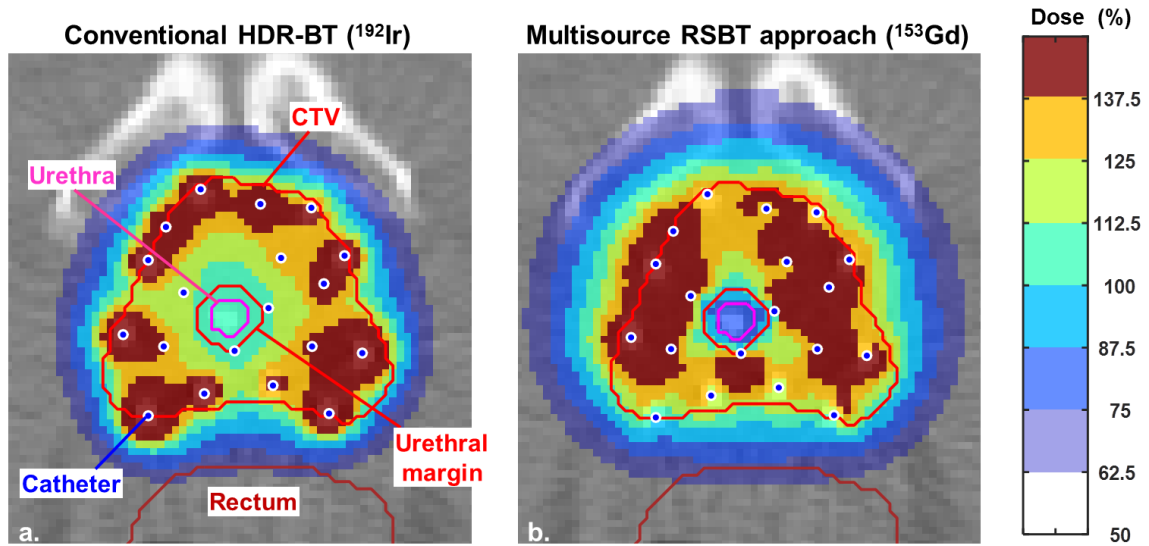
Figure 21: Dose distribution for 1-mm urethral margin of (a) [192]Ir based HDR-BT and (b) [153]Gd based I-RSBT with multisource RSBT apparatus sampled onto a CT scan of a prostate cancer patient.
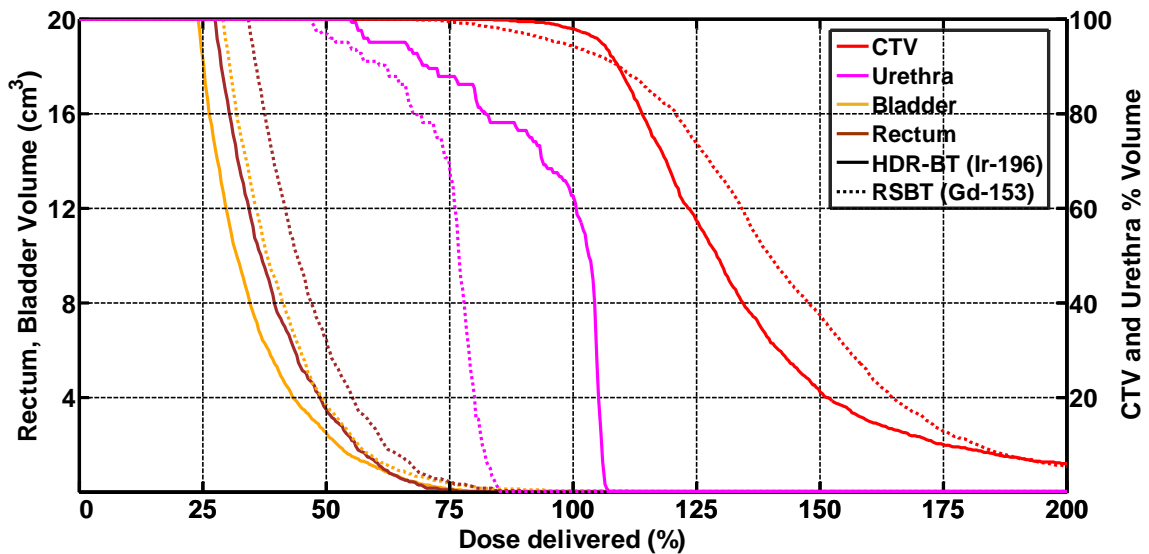
Figure 22: Dose-volume histograms for conventional ^{192}Ir based HDR-BT and [153]Gd based I-RSBT with multisource RSBT apparatus for urethral margin of 1 mm.
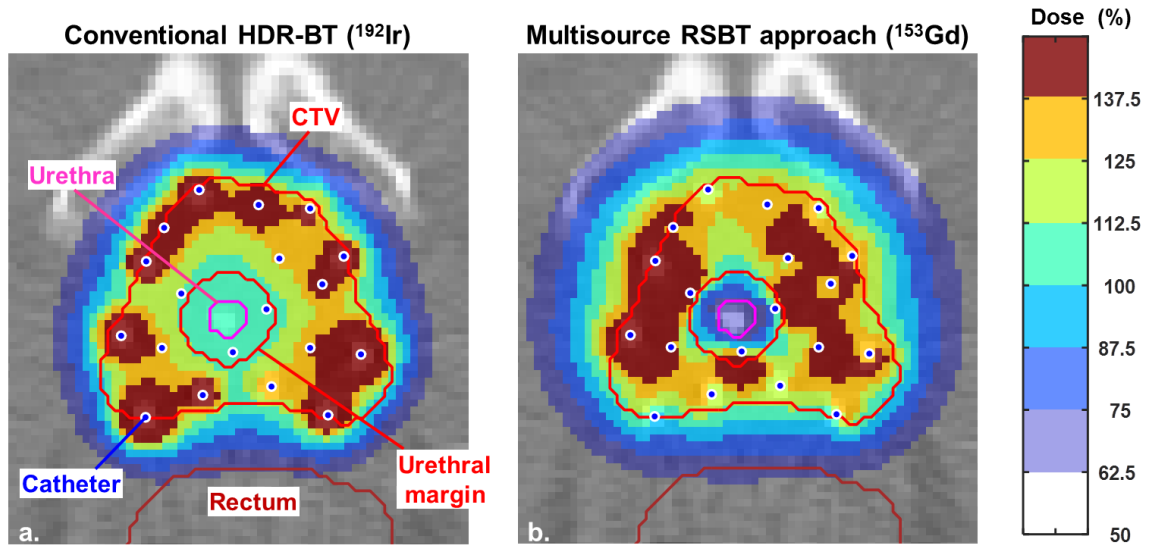
Figure 23: Dose distribution for 3-mm urethral margin of (a) [192]Ir based HDR-BT and (b) [153]Gd based I-RSBT with multisource RSBT apparatus sampled onto a CT scan of a prostate cancer patient.
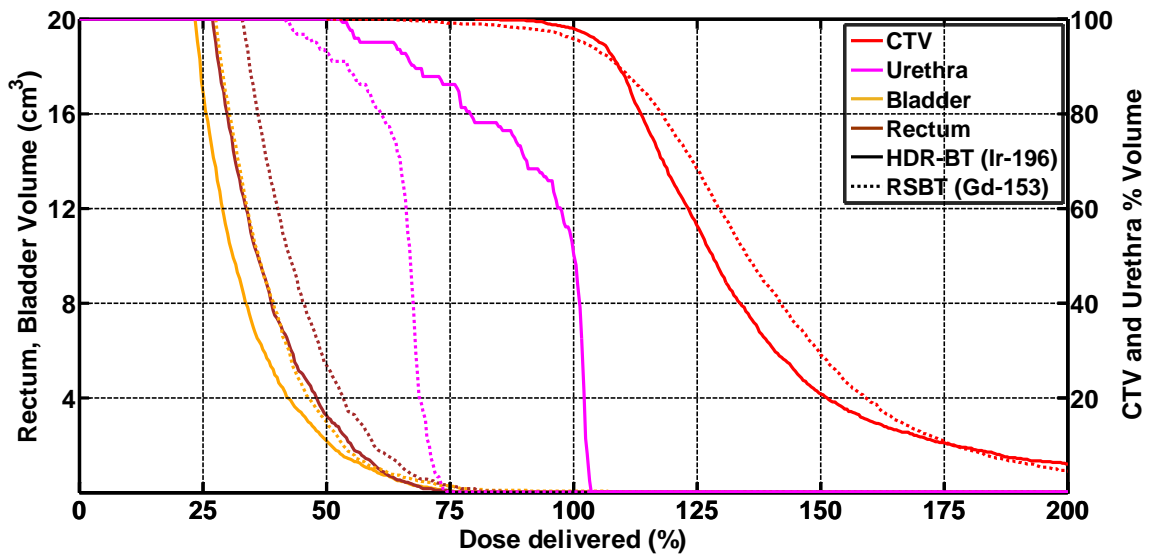
Figure 24: Dose-volume histograms for conventional ^{192}Ir based HDR-BT and [153]Gd based I-RSBT with multisource RSBT apparatus for urethral margin of 3 mm.
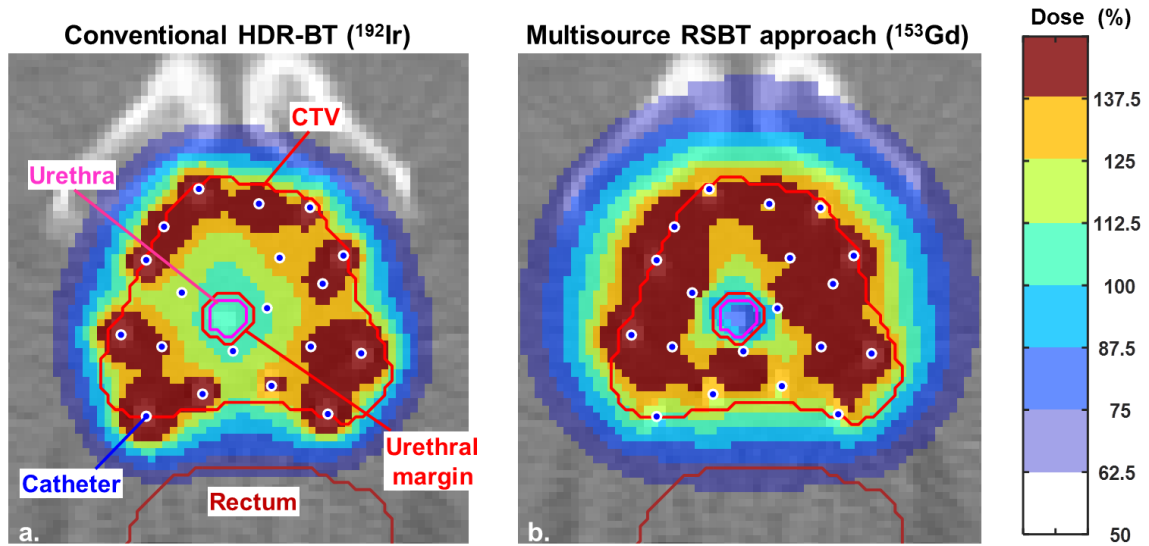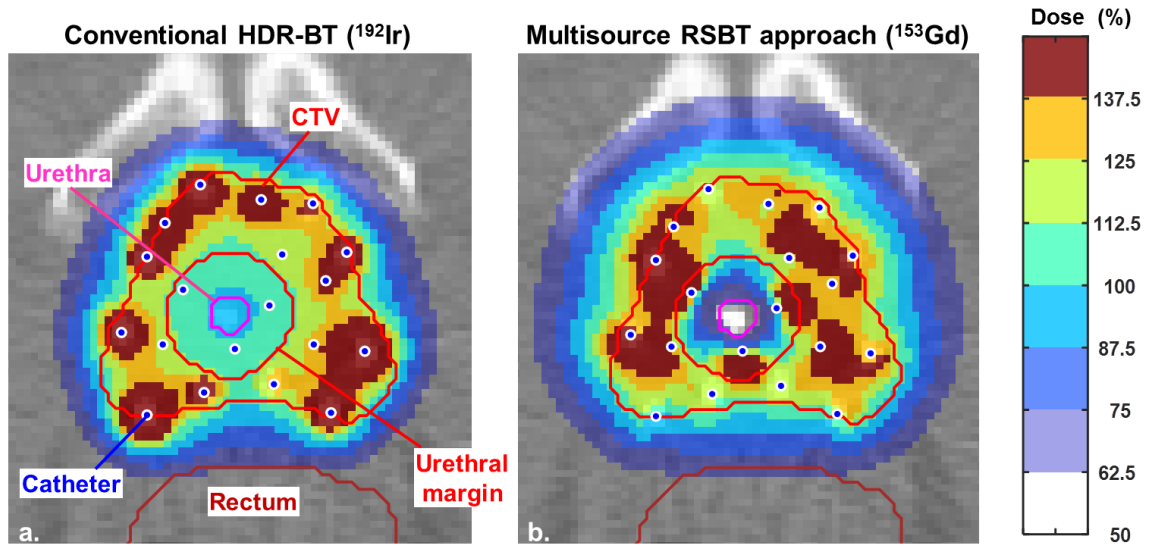
Figure 25: Dose distribution for 5-mm urethral margin of (a) [192]Ir based HDR-BT and (b) [153]Gd based I-RSBT with multisource RSBT apparatus sampled onto a CT scan of a prostate cancer patient.
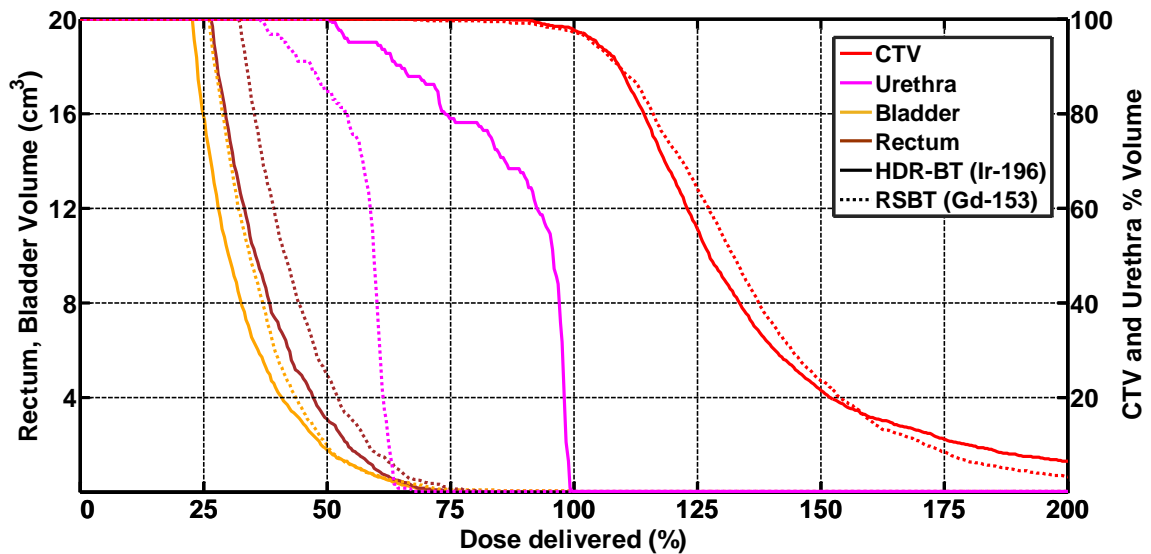
Figure 26: Dose-volume histograms for conventional ^{192}Ir based HDR-BT and [153]Gd based I-RSBT with multisource RSBT apparatus for urethral margin of 5 mm.

For the same CTV D_{90} of the patient considered and 3 mm urethral margin, the planned treatment with the multisource RSBT apparatus reduced urethral $D_{0.1cc}$ below that of ^{192}Ir based HDR-BT by 31% relative to the prescribed dose of 100%. For the same urethral dose gradient volume, peri-apical $D_{0.1cc}$ was reduced by 24.85%. The urethral margins were included in the models as relaxed prescription dose constraints in order to provide a spatial location for the dose gradient about the urethra. Further, the delivery time of 20 Gy to the CTV of the case considered treated with HDR-BT using a 370 GBq ^{192}Ir source was 15.8 minutes while that using RSBT with nineteen 62.4 GBq ^{153}Gd sources was 122 minutes.

7.2 Sensitivity analysis

Plots of the urethral $D_{0.1cc}$ and CTV D_{90} percentage variations as a function of emission direction rotational error and catheter positional error are shown in **Figure 27a** and **Figure 27b**, respectively.
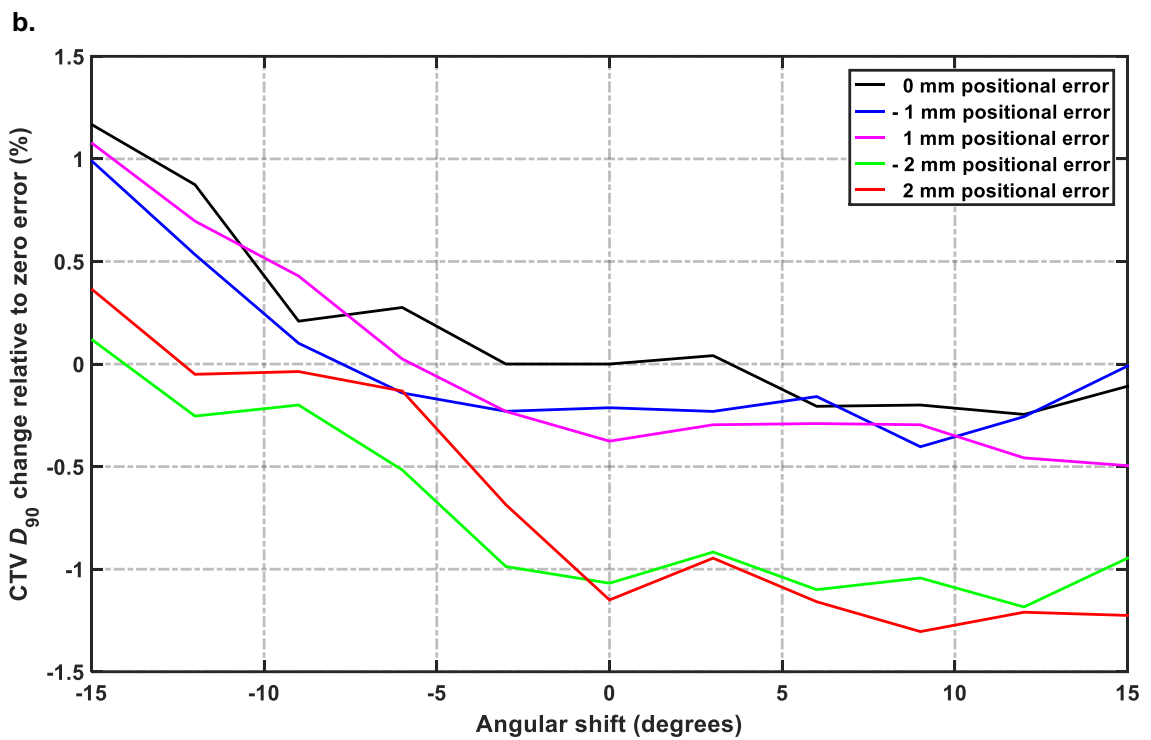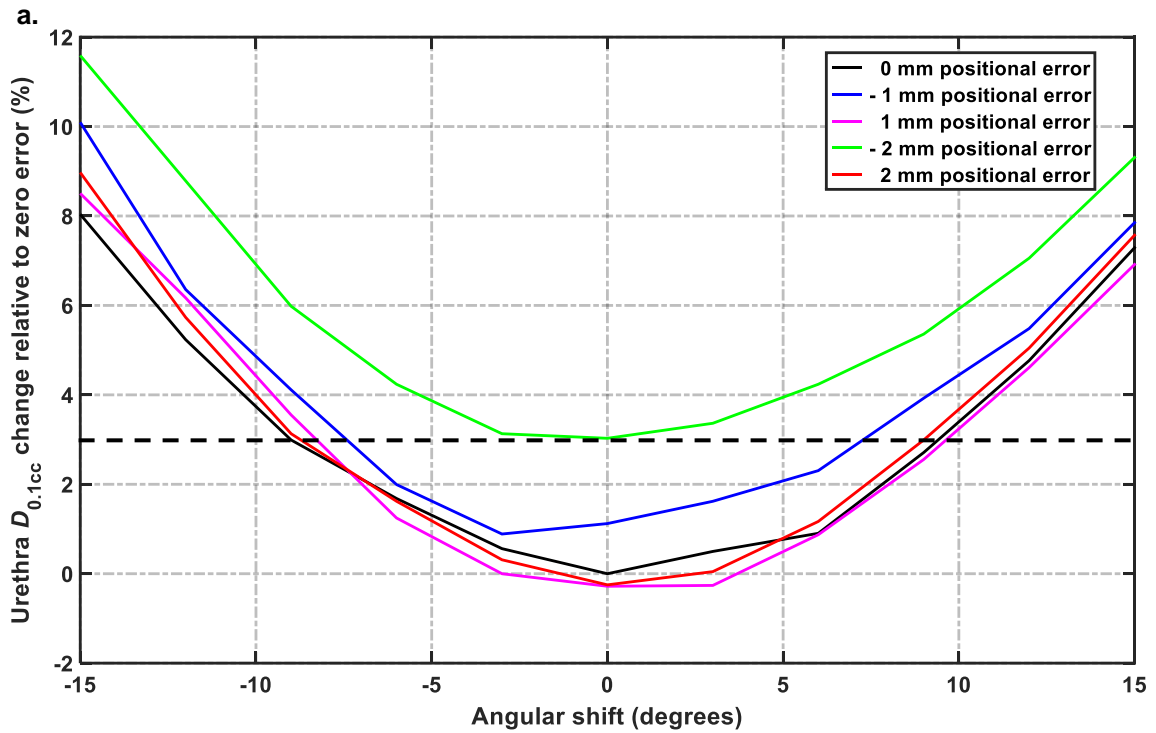
Figure 27: Dosimetric impact of positional and rotational uncertainty of catheters on (a) urethral $D_{0.1cc}$ and (b) CTV D_{90}. The dashed line in (a) represents 3% error which is considered as the tolerable accuracy.

With the increasing values of angular deviation of the source's emission direction from the ideal state of zero degree error, urethral $D_{0.1cc}$ value increases as shown in **Figure 27(a)**. The systematic angular error of 15° from the baseline increased the urethral $D_{0.1cc}$ by 8%. For the case considered, urethral $D_{0.1cc}$ increased by 3% with 2 mm positional error. **Figure 27(a)** shows that when all of the catheters have 2 mm longitudinal errors and are rotated 15° incorrectly, there is an 11.6% increase in urethral $D_{0.1cc}$. **Figure 27(b)** shows that the catheters' emission direction error could either increase or decrease the value of CTV D_{90}. For the same urethral dose gradient volume peri-apical $D_{0.1cc}$ was reduced by 25%. The delivery time for 20 Gy to the CTV for the case considered was 15.8 min with HDR-BT using a 370 GBq ^{192}Ir source and 121.7 min with RSBT.

7.3 Conceptual prototype

One of the goals of this project is to design and manufacture a prototype device that will be able to rotate several threaded shafts simultaneously and with the same angle by translating a moving template between two stationary templates. The shafts will finally incorporate other parts as explained in **Figure 15** and **Figure 16**. Peripheral walls of the shafts and the interior wall of the holes machined into the moving template have the same threading pattern. As the moving template is translated back and forth, the threadings contacts force the shafts to rotate. **Figure 28a** and **Figure 28b** shows the CAD model and the manufactured prototype of the angular drive mechanism, respectively, which includes only five threaded shafts. The role of the guide rods is to hold the moving template along the axis of rotation of the shafts while the moving template is free to slide back and forth along them. The guide rods are also held in place by means of the two

63

stationary templates. In this prototype the moving template and the rotating shafts are generated as 3-D printed plastic with 20 µm resolution. The rotating shafts printed for this prototype are threaded to provide a pitch with 10 cm translation per shaft rotation (1 mm per 3.6° rotation), which will be sufficient to balance the tradeoffs between rotational accuracy, apparatus length, and resistive force exerted on the moving template by the shafts during motion.
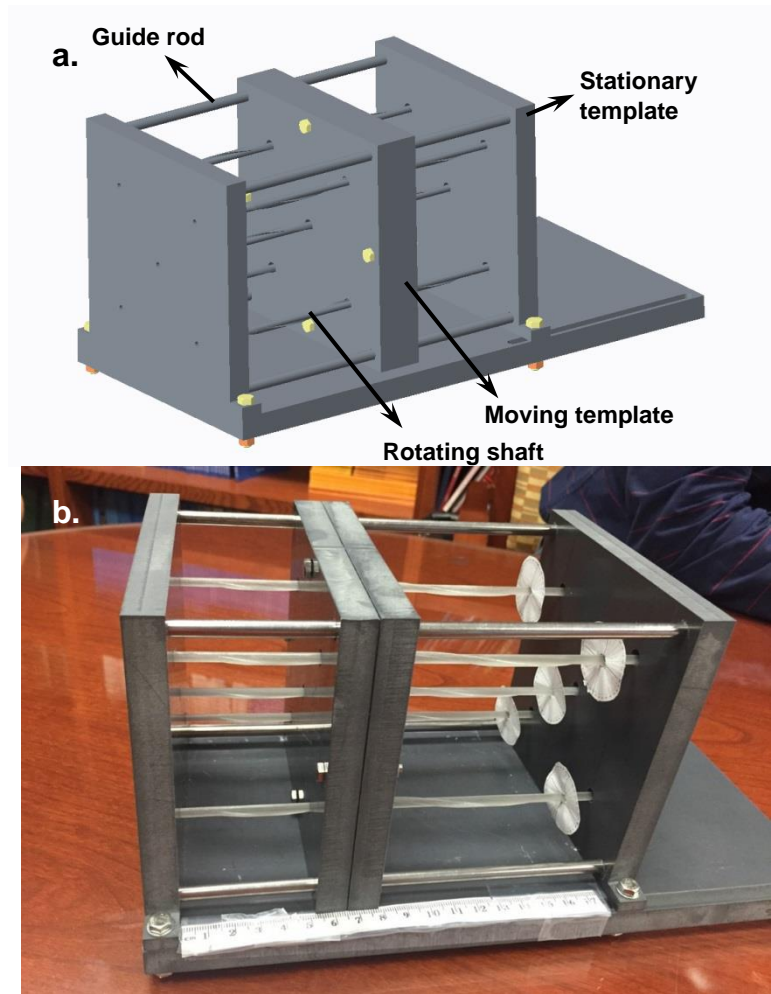
Figure 28: The assembled CAD model **(a)** and the built prototype **(b)** of the angular drive mechanism of multisource RSBT apparatus consisting of the moving template and five rotating threaded shafts.

8 DISCUSSION

The urethral margins of 0, 1, 3, and 5 mm were added to the boundary of the urethra for the case considered, irrespective of the prostate size, and no constraints were applied to the dose inside the margin in the treatment planning process. The resulting dose distributions indicate that RSBT with the proposed multisource apparatus induced cold spots only inside and adjacent to the urethra, which is desirable in terms of minimizing normal tissue toxicity. Besides that, the DVH plots exhibit a shift to the left in the urethral DVH relative to that of conventional HDR-BT technique. However the physician would need to select the appropriate margin for a given patient.

The proposed mechanism in **Figure 17** offers a number of unique attributes. First, the dimensions of the unit are small enough that the system can be used in common procedure rooms. Second, as the connectors have the freedom to move longitudinally prior to the connection between the angular drive mechanism and the needles, the depth of needles entry into the patient's perineum does not matter. Third, although the angular drive mechanism dictates all of the 20 emission windows in the patient to be at the same direction during the irradiation process, the independent depth control for each shielded source enabled by the multisource remote afterloader provides efficient treatments. Fourth, the control over longitudinal translation and the control over rotation of the shielded sources into the needles are independent.

All of the shielded sources' aluminium emission windows are oriented in the same emission direction at the same time during the irradiation process. Therefore the delivery scheme would be based on completing all of the dwell positions of all the catheters in a single rotational angle and then switching to the next rotational angle by means of translating the moving template one sixteenth of the distance needed to create a single full

65

rotation of the catheters. Accordingly the total amount of time spent on a single emission direction is dictated by the catheter with the longest cumulative dwell time for that direction. The treatment time for delivering RSBT dose with multisource RSBT apparatus shows an increase by a factor of about 7 relative to the conventional HDR-BT treatment time due to the lower dose rate of ^{153}Gd relative to ^{192}Ir. As all of the shielded sources have the same orientation in a single translational position of the moving template, inter-source attenuation is a potential concern with the proposed approach. Our strategy for addressing this issue is to develop a delivery optimization approach in which the longitudinal positions for all of the sources for a given delivery angle are intelligently ordered in time to minimize inter-source attenuation.

The precision of radiation dose delivery of multisource RSBT apparatus as well as safe delivery of high radiation doses to the prostate should be guaranteed during the treatment. For the presented mechanism it is dependent on the precise longitudinal and rotational positioning of the catheters during the irradiation process in which the catheter angles are simultaneously incremented. Therefore, a catheter position monitoring and control system is needed in order to empirically verify that the catheter angles and depths are within the required tolerances for safe radiation delivery. This is accomplished with a mechanism using feedback from multiple cameras to measure and correct for catheter longitudinal and angular positioning errors in real time.

It is expected that RSBT delivery would take place under trans-rectal ultrasound (TRUS) guidance. The current version of the RSBT angular drive mechanism is designed to demonstrate mechanical feasibility of the approach and is not yet compatible with a commercially available TRUS system. It is expected that modifications can be

66

successfully made to the angular drive mechanism to enable TRUS usage, and the associated workflows can later be defined.

As the focus of this study is on presenting a novel apparatus for controlling multiple shielded radiation sources simultaneously in terms of both depth and angle, only a single previously treated prostate cancer patient was considered as the case study. However that is a limitation in our approach and an extensive (> 20 patients) treatment planning study is necessary to be conducted in order to thoroughly evaluate the proposed technique.

In conclusion, the proposed multisource RSBT delivery apparatus in conjunction with multiple nitinol catheter-mounted platinum-shielded ^{153}Gd sources enables a mechanically feasible urethra-sparing treatment technique for prostate cancer in a clinically reasonable timeframe of two hours.

9 CONCLUSION

The target conformity of conventional HDR-BT dose distributions is restricted based on the geometrical constraints imposed by the position and shape of the tube-shaped applicators, as well as the radially-symmetric radiation dose distributions produced by the radiation sources. Dose distribution conformity for cervical and prostate cancer can be significantly improved relative to conventional HDR-BT through the use of RSBT. With RSBT, radiation sources are partially shielded and have the freedom to rotate in an optimized fashion such that radiation dose is directed away from sensitive structures and into the targeted tissue. RSBT will advance brachytherapy treatment with superior dose conformity, while maintaining the inherent accuracy, flexibility, and insensitivity to patient motion of conventional HDR-BT, as well as enable dose escalation without compromising organ at risk (OAR) sparing. These improvements are expected to result in a clinically-relevant improvement in the outcomes of patients treated with RSBT relative to conventional HDR-BT.

The idea of RSBT was first conceived more than a decade ago. However, the considerable challenges associated with its clinical implementation have delayed its application in brachytherapy treatment planning of cervical and prostate cancer, necessitating proposing novel, innovative, and clinically realizable techniques and mechanisms. New radiation sources introduced in recent years such as ^{153}Gd and the electronic-based source of Xoft Axxent^{TM} are practical and suitable alternatives to conventional ^{192}Ir sources, which are difficult or impractical to shield effectively given the limited space available inside the applicators used for brachytherapy of cervical and prostate cancer. Efficient and feasible mechanical RSBT delivery solutions have become major limiting factors for the clinical implementation of this concept. We proposed to

68

develop novel mechanisms in order to bring RSBT into the clinic for the treatment of cervical and prostate cancer. The overall hypothesis driving this dissertation is that: The helical RSBT approach for treating cervical cancer and the multi-catheter RSBT approach for treating prostate cancer, powered with novel radiation sources amenable to shielding, are clinically feasible techniques that dosimetrically outperform conventional brachytherapy methods while minimizing damage to healthy tissues inside and/or adjacent to the target.

The helical RSBT method and the multi-catheter RSBT approach overcome the technical and clinical barriers to implementation of the previously proposed RSBT ideas for cervical and prostate cancer, respectively, enabling the delivery of deliberately asymmetric, tumor-conformal, and OAR-minimally-invasive dose distributions with higher target dose. The two novel techniques proposed in this work will lay the technological framework for clinical RSBT implementation of cervical and prostate cancer radiation-based treatment and will provide a rigorous estimate of the advantages that RSBT can provide for thousands of patients over conventional HDR-BT. We expect the improvement achieved by these novel RSBT techniques and mechanisms in the delivered dose distributions will reduce the probability of prostate and cervical cancer patients experiencing treatment-based side effects, improving quality of life.

REFERENCES

1. L. A. Torre, F. Bray, R. L. Siegel, J. Ferlay, J. Lortet-Tieulent and A. Jemal, "Global cancer statistics, 2012," CA: a cancer journal for clinicians **65**, 87-108 (2015).

2. E. K. Hansen and M. Roach, "Handbook of evidence-based radiation oncology," (Springer, New York, NY, 2007), pp. 499-512.

3. L. S. Massad, M. H. Einstein, W. K. Huh, H. A. Katki, W. K. Kinney, M. Schiffman, D. Solomon, N. Wentzensen, H. W. Lawson and A. C. G. Conference, "2012 updated consensus guidelines for the management of abnormal cervical cancer screening tests and cancer precursors," Obstetrics and gynecology **121**, 829-846 (2013).

4. J. M. Walboomers, M. V. Jacobs, M. M. Manos, F. X. Bosch, J. A. Kummer, K. V. Shah, P. J. Snijders, J. Peto, C. J. Meijer and N. Munoz, "Human papillomavirus is a necessary cause of invasive cervical cancer worldwide," The Journal of pathology **189**, 12-19 (1999).

5. F. X. Bosch, A. Lorincz, N. Munoz, C. J. Meijer and K. V. Shah, "The causal relation between human papillomavirus and cervical cancer," Journal of clinical pathology **55**, 244-265 (2002).

6. R. Siegel, E. Ward, O. Brawley and A. Jemal, "Cancer statistics, 2011: the impact of eliminating socioeconomic and racial disparities on premature cancer deaths," CA: a cancer journal for clinicians **61**, 212-236 (2011).

7. S. Pecorelli, L. Zigliani and F. Odicino, "Revised FIGO staging for carcinoma of the cervix," International journal of gynaecology and obstetrics: the official organ of the International Federation of Gynaecology and Obstetrics **105**, 107-108 (2009).

8. S. M. Lewis, S. R. Dirksen, M. M. Heitkemper, L. Bucher and M. Harding, *Medical-surgical nursing : assessment and management of clinical problems*, Ninth edition. ed. (Elsevier/Mosby, St. Louis, Missouri, 2014).

70

9. H. M. Keys, B. N. Bundy, F. B. Stehman, L. I. Muderspach, W. E. Chafe, C. L. Suggs, 3rd, J. L. Walker and D. Gersell, "Cisplatin, radiation, and adjuvant hysterectomy compared with radiation and adjuvant hysterectomy for bulky stage IB cervical carcinoma," The New England journal of medicine **340**, 1154-1161 (1999).

10. J. C. Dimopoulos, P. Petrow, K. Tanderup, P. Petric, D. Berger, C. Kirisits, E. M. Pedersen, E. van Limbergen, C. Haie-Meder and R. Potter, "Recommendations from Gynaecological (GYN) GEC-ESTRO Working Group (IV): Basic principles and parameters for MR imaging within the frame of image based adaptive cervix cancer brachytherapy," Radiotherapy and oncology : journal of the European Society for Therapeutic Radiology and Oncology **103**, 113-122 (2012).

11. R. Potter, P. Georg, J. C. Dimopoulos, M. Grimm, D. Berger, N. Nesvacil, D. Georg, M. P. Schmid, A. Reinthaller, A. Sturdza and C. Kirisits, "Clinical outcome of protocol based image (MRI) guided adaptive brachytherapy combined with 3D conformal radiotherapy with or without chemotherapy in patients with locally advanced cervical cancer," Radiotherapy and oncology : journal of the European Society for Therapeutic Radiology and Oncology **100**, 116-123 (2011).

12. L. Coia, M. Won, R. Lanciano, V. A. Marcial, K. Martz and G. Hanks, "The Patterns of Care Outcome Study for cancer of the uterine cervix. Results of the Second National Practice Survey," Cancer **66**, 2451-2456 (1990).

13. R. M. Lanciano, M. Won, L. R. Coia and G. E. Hanks, "Pretreatment and treatment factors associated with improved outcome in squamous cell carcinoma of the uterine cervix: a final report of the 1973 and 1978 patterns of care studies," International journal of radiation oncology, biology, physics **20**, 667-676 (1991).

14. R. Mohan, I. Y. Ding, J. Toraskar, C. Chui, L. L. Anderson and D. Nori, "Computation of radiation dose distributions for shielded cervical applicators," International journal of radiation oncology, biology, physics **11**, 823-830 (1985).

71

15. M. Pinn-Bingham, A. A. Puthawala, A. M. Syed, A. Sharma, P. Disaia, M. Berman, K. S. Tewari, L. Randall-Whitis, U. Mahmood, N. Ramsinghani, J. Kuo, W. P. Chen and C. E. McLaren, "Outcomes of high-dose-rate interstitial brachytherapy in the treatment of locally advanced cervical cancer: long-term results," International journal of radiation oncology, biology, physics **85**, 714-720 (2013).

16. I. C. Hsu, J. Speight, J. Hai, E. Vigneault, T. Phillips and J. Pouliot, "A comparison between tandem and ovoids and interstitial gynecologic template brachytherapy dosimetry using a hypothetical computer model," International journal of radiation oncology, biology, physics **52**, 538-543 (2002).

17. C. Kirisits, S. Lang, J. Dimopoulos, D. Berger, D. Georg and R. Potter, "The Vienna applicator for combined intracavitary and interstitial brachytherapy of cervical cancer: design, application, treatment planning, and dosimetric results," International journal of radiation oncology, biology, physics **65**, 624-630 (2006).

18. R. Potter, C. Haie-Meder, E. Van Limbergen, I. Barillot, M. De Brabandere, J. Dimopoulos, I. Dumas, B. Erickson, S. Lang, A. Nulens, P. Petrow, J. Rownd, C. Kirisits and G. E. W. Group, "Recommendations from gynaecological (GYN) GEC ESTRO working group (II): concepts and terms in 3D image-based treatment planning in cervix cancer brachytherapy-3D dose volume parameters and aspects of 3D image-based anatomy, radiation physics, radiobiology," Radiotherapy and oncology : journal of the European Society for Therapeutic Radiology and Oncology **78**, 67-77 (2006).

19. A. N. Viswanathan, J. Dimopoulos, C. Kirisits, D. Berger and R. Potter, "Computed tomography versus magnetic resonance imaging-based contouring in cervical cancer brachytherapy: results of a prospective trial and preliminary guidelines for standardized contours," International journal of radiation oncology, biology, physics **68**, 491-498 (2007).

20. J. C. Dimopoulos, C. Kirisits, P. Petric, P. Georg, S. Lang, D. Berger and R. Potter, "The Vienna applicator for combined intracavitary and interstitial brachytherapy of cervical cancer: clinical feasibility and preliminary results," International journal of radiation oncology, biology, physics **66**, 83-90 (2006).

72

21. K. S. Chao, J. F. Williamson, P. W. Grigsby and C. A. Perez, "Uterosacral space involvement in locally advanced carcinoma of the uterine cervix," International journal of radiation oncology, biology, physics **40**, 397-403 (1998).

22. R. Potter, J. Dimopoulos, P. Georg, S. Lang, C. Waldhausl, N. Wachter-Gerstner, H. Weitmann, A. Reinthaller, T. H. Knocke, S. Wachter and C. Kirisits, "Clinical impact of MRI assisted dose volume adaptation and dose escalation in brachytherapy of locally advanced cervix cancer," Radiotherapy and oncology : journal of the European Society for Therapeutic Radiology and Oncology **83**, 148-155 (2007).

23. E. Y. Huang, L. M. Sun, H. Lin, J. H. Lan, C. C. Chanchien, Y. J. Huang, C. Y. Wang and C. J. Wang, "A prospective cohort study to compare treatment results between 2 fractionation schedules of high-dose-rate intracavitary brachytherapy (HDR-ICBT) in patients with cervical cancer," International journal of radiation oncology, biology, physics **85**, 123-128 (2013).

24. J. C. Dimopoulos, S. Lang, C. Kirisits, E. F. Fidarova, D. Berger, P. Georg, W. Dorr and R. Potter, "Dose-volume histogram parameters and local tumor control in magnetic resonance image-guided cervical cancer brachytherapy," International journal of radiation oncology, biology, physics **75**, 56-63 (2009).

25. J. C. Dimopoulos, R. Potter, S. Lang, E. Fidarova, P. Georg, W. Dorr and C. Kirisits, "Dose-effect relationship for local control of cervical cancer by magnetic resonance image-guided brachytherapy," Radiotherapy and oncology : journal of the European Society for Therapeutic Radiology and Oncology **93**, 311-315 (2009).

26. I. M. Jurgenliemk-Schulz, R. J. Tersteeg, J. M. Roesink, S. Bijmolt, C. N. Nomden, M. A. Moerland and A. A. de Leeuw, "MRI-guided treatment-planning optimisation in intracavitary or combined intracavitary/interstitial PDR brachytherapy using tandem ovoid applicators in locally advanced cervical cancer," Radiotherapy and oncology : journal of the European Society for Therapeutic Radiology and Oncology **93**, 322-330 (2009).

27. K. Tanderup, S. K. Nielsen, G. B. Nyvang, E. M. Pedersen, L. Rohl, T. Aagaard, L. Fokdal and J. C. Lindegaard, "From point A to the sculpted pear: MR image guidance significantly improves tumour dose and sparing of organs at risk in brachytherapy of cervical cancer," Radiotherapy and oncology : journal of the European Society for Therapeutic Radiology and Oncology **94**, 173-180 (2010).

28. C. L. Holloway, M. L. Racine, R. A. Cormack, D. A. O'Farrell and A. N. Viswanathan, "Sigmoid dose using 3D imaging in cervical-cancer brachytherapy," Radiotherapy and oncology : journal of the European Society for Therapeutic Radiology and Oncology **93**, 307-310 (2009).

29. S. Kato, D. N. Tran, T. Ohno, T. Nakano, H. Kiyohara, Y. Ohkubo and T. Kamada, "CT-based 3D dose-volume parameter of the rectum and late rectal complication in patients with cervical cancer treated with high-dose-rate intracavitary brachytherapy," Journal of radiation research **51**, 215-221 (2010).

30. P. Georg, R. Potter, D. Georg, S. Lang, J. C. Dimopoulos, A. E. Sturdza, D. Berger, C. Kirisits and W. Dorr, "Dose effect relationship for late side effects of the rectum and urinary bladder in magnetic resonance image-guided adaptive cervix cancer brachytherapy," International journal of radiation oncology, biology, physics **82**, 653-657 (2012).

31. M. J. Webster, S. Devic, T. Vuong, D. Yup Han, J. C. Park, D. Scanderbeg, J. Lawson, B. Song, W. Tyler Watkins, T. Pawlicki and W. Y. Song, "Dynamic modulated brachytherapy (DMBT) for rectal cancer," Medical physics **40**, 011718 (2013).

32. W. Yang, Y. Kim, X. Wu, Q. Song, Y. Liu, S. K. Bhatia, W. Sun and R. T. Flynn, "Rotating-shield brachytherapy for cervical cancer," Physics in medicine and biology **58**, 3931-3941 (2013).

33. Y. Liu, R. T. Flynn, Y. Kim and X. Wu, "Asymmetric dose-volume optimization with smoothness control for rotating-shield brachytherapy," Medical physics **41**, 111709 (2014).

34. H. Dadkhah, Y. Kim, X. Wu and R. T. Flynn, "Multihelix rotating shield brachytherapy for cervical cancer," Medical physics **42**, 6579-6588 (2015).

35. Y. Liu, R. T. Flynn, Y. Kim, H. Dadkhah, S. K. Bhatia, J. M. Buatti, W. Xu and X. Wu, "Paddle-based rotating-shield brachytherapy," Medical physics **42**, 5992-6003 (2015).

36. D. Y. Han, M. J. Webster, D. J. Scanderbeg, C. Yashar, D. Choi, B. Song, S. Devic, A. Ravi and W. Y. Song, "Direction-modulated brachytherapy for high-dose-rate treatment of cervical cancer. I: theoretical design," International journal of radiation oncology, biology, physics **89**, 666-673 (2014).

37. D. Y. Han, H. Safigholi, A. Soliman, A. Ravi, E. Leung, D. J. Scanderbeg, Z. Liu, A. Owrangi and W. Y. Song, "Direction Modulated Brachytherapy for Treatment of Cervical Cancer. II: Comparative Planning Study With Intracavitary and Intracavitary-Interstitial Techniques," International journal of radiation oncology, biology, physics **96**, 440-448 (2016).

38. A. Dickler and K. Dowlatshahi, "Xoft Axxent electronic brachytherapy," Expert review of medical devices **6**, 27-31 (2009).

39. M. Joiner and A. v. d. Kogel, *Basic clinical radiobiology*, 4th ed. (Hodder Arnold ;, London, 2009).

40. C. Haie-Meder, R. Potter, E. Van Limbergen, E. Briot, M. De Brabandere, J. Dimopoulos, I. Dumas, T. P. Hellebust, C. Kirisits, S. Lang, S. Muschitz, J. Nevinson, A. Nulens, P. Petrow, N. Wachter-Gerstner and G. E. C. E. W. G. Gynaecological, "Recommendations from Gynaecological (GYN) GEC-ESTRO Working Group (I): concepts and terms in 3D image based 3D treatment planning in cervix cancer brachytherapy with emphasis on MRI assessment of GTV and CTV," Radiotherapy and oncology : journal of the European Society for Therapeutic Radiology and Oncology **74**, 235-245 (2005).

41. R. Nath, L. L. Anderson, G. Luxton, K. A. Weaver, J. F. Williamson and A. S. Meigooni, "Dosimetry of interstitial brachytherapy sources: recommendations of the AAPM Radiation Therapy Committee Task Group No. 43. American Association of Physicists in Medicine," Medical physics **22**, 209-234 (1995).

75

42. M. J. Rivard, B. M. Coursey, L. A. DeWerd, W. F. Hanson, M. S. Huq, G. S. Ibbott, M. G. Mitch, R. Nath and J. F. Williamson, "Update of AAPM Task Group No. 43 Report: A revised AAPM protocol for brachytherapy dose calculations," Medical physics **31**, 633-674 (2004).

43. M. J. Rivard, S. D. Davis, L. A. DeWerd, T. W. Rusch and S. Axelrod, "Calculated and measured brachytherapy dosimetry parameters in water for the Xoft Axxent X-Ray Source: an electronic brachytherapy source," Medical physics **33**, 4020-4032 (2006).

44. Y. Liu, R. T. Flynn, W. Yang, Y. Kim, S. K. Bhatia, W. Sun and X. Wu, "Rapid emission angle selection for rotating-shield brachytherapy," Medical physics **40**, 051720 (2013).

45. D. M. Shepard, G. H. Olivera, P. J. Reckwerdt and T. R. Mackie, "Iterative approaches to dose optimization in tomotherapy," Physics in medicine and biology **45**, 69-90 (2000).

46. A. Jemal, F. Bray, M. M. Center, J. Ferlay, E. Ward and D. Forman, "Global cancer statistics," CA: a cancer journal for clinicians **61**, 69-90 (2011).

47. R. L. Siegel, K. D. Miller and A. Jemal, "Cancer statistics, 2015," CA: a cancer journal for clinicians **65**, 5-29 (2015).

48. C. E. DeSantis, C. C. Lin, A. B. Mariotto, R. L. Siegel, K. D. Stein, J. L. Kramer, R. Alteri, A. S. Robbins and A. Jemal, "Cancer treatment and survivorship statistics, 2014," CA: a cancer journal for clinicians **64**, 252-271 (2014).

49. J. Li, J. A. Djenaba, A. Soman, S. H. Rim and V. A. Master, "Recent trends in prostate cancer incidence by age, cancer stage, and grade, the United States, 2001-2007," Prostate cancer **2012**, 691380 (2012).

50. M. J. Hayat, N. Howlader, M. E. Reichman and B. K. Edwards, "Cancer statistics, trends, and multiple primary cancer analyses from the Surveillance, Epidemiology, and End Results (SEER) Program," The oncologist **12**, 20-37 (2007).

51. D. P. Dearnaley, M. R. Sydes, J. D. Graham, E. G. Aird, D. Bottomley, R. A. Cowan, R. A. Huddart, C. C. Jose, J. H. Matthews, J. Millar, A. R. Moore, R. C. Morgan, J. M. Russell, C. D. Scrase, R. J. Stephens, I. Syndikus, M. K. Parmar and R. T. collaborators, "Escalated-dose versus standard-dose conformal radiotherapy in prostate cancer: first results from the MRC RT01 randomised controlled trial," The Lancet. Oncology **8**, 475-487 (2007).

52. M. Menon, A. Tewari, B. Baize, B. Guillonneau and G. Vallancien, "Prospective comparison of radical retropubic prostatectomy and robot-assisted anatomic prostatectomy: the Vattikuti Urology Institute experience," Urology **60**, 864-868 (2002).

53. K. A. Roehl, M. Han, C. G. Ramos, J. A. Antenor and W. J. Catalona, "Cancer progression and survival rates following anatomical radical retropubic prostatectomy in 3,478 consecutive patients: long-term results," The Journal of urology **172**, 910-914 (2004).

54. M. J. Zelefsky, S. A. Leibel, P. B. Gaudin, G. J. Kutcher, N. E. Fleshner, E. S. Venkatramen, V. E. Reuter, W. R. Fair, C. C. Ling and Z. Fuks, "Dose escalation with three-dimensional conformal radiation therapy affects the outcome in prostate cancer," International journal of radiation oncology, biology, physics **41**, 491-500 (1998).

55. L. Potters, E. A. Klein, M. W. Kattan, C. A. Reddy, J. P. Ciezki, A. M. Reuther and P. A. Kupelian, "Monotherapy for stage T1-T2 prostate cancer: radical prostatectomy, external beam radiotherapy, or permanent seed implantation," Radiotherapy and oncology : journal of the European Society for Therapeutic Radiology and Oncology **71**, 29-33 (2004).

56. M. Roach, 3rd, G. Hanks, H. Thames, Jr., P. Schellhammer, W. U. Shipley, G. H. Sokol and H. Sandler, "Defining biochemical failure following radiotherapy with or without hormonal therapy in men with clinically localized prostate cancer: recommendations of the RTOG-ASTRO Phoenix Consensus Conference," International journal of radiation oncology, biology, physics **65**, 965-974 (2006).

77

57. R. E. Peschel, Z. Chen, K. Roberts and R. Nath, "Long-term complications with prostate implants: iodine-125 vs. palladium-103," Radiation oncology investigations **7**, 278-288 (1999).

58. R. G. Stock, J. A. Cesaretti and N. N. Stone, "Disease-specific survival following the brachytherapy management of prostate cancer," International journal of radiation oncology, biology, physics **64**, 810-816 (2006).

59. S. Voulgaris, J. P. Nobes, R. W. Laing and S. E. Langley, "State-of-the-art: prostate LDR brachytherapy," Prostate cancer and prostatic diseases **11**, 237-240 (2008).

60. I. S. Grills, A. A. Martinez, M. Hollander, R. Huang, K. Goldman, P. Y. Chen and G. S. Gustafson, "High dose rate brachytherapy as prostate cancer monotherapy reduces toxicity compared to low dose rate palladium seeds," The Journal of urology **171**, 1098-1104 (2004).

61. Y. Yoshioka, K. Konishi, I. Sumida, Y. Takahashi, F. Isohashi, T. Ogata, M. Koizumi, H. Yamazaki, N. Nonomura, A. Okuyama and T. Inoue, "Monotherapeutic high-dose-rate brachytherapy for prostate cancer: five-year results of an extreme hypofractionation regimen with 54 Gy in nine fractions," International journal of radiation oncology, biology, physics **80**, 469-475 (2011).

62. M. Barkati, S. G. Williams, F. Foroudi, K. H. Tai, S. Chander, S. van Dyk, A. See and G. M. Duchesne, "High-dose-rate brachytherapy as a monotherapy for favorable-risk prostate cancer: a Phase II trial," International journal of radiation oncology, biology, physics **82**, 1889-1896 (2012).

63. M. Ghilezan, A. Martinez, G. Gustason, D. Krauss, J. V. Antonucci, P. Chen, J. Fontanesi, M. Wallace, H. Ye, A. Casey, E. Sebastian, L. Kim and A. Limbacher, "High-dose-rate brachytherapy as monotherapy delivered in two fractions within one day for favorable/intermediate-risk prostate cancer: preliminary toxicity data," International journal of radiation oncology, biology, physics **83**, 927-932 (2012).

64. P. Hoskin, A. Rojas, G. Lowe, L. Bryant, P. Ostler, R. Hughes, J. Milner and H. Cladd, "High-dose-rate brachytherapy alone for localized prostate cancer in patients at moderate or high risk of biochemical recurrence," International journal of radiation oncology, biology, physics **82**, 1376-1384 (2012).

65. D. J. Demanes and M. I. Ghilezan, "High-dose-rate brachytherapy as monotherapy for prostate cancer," Brachytherapy **13**, 529-541 (2014).

66. Y. Yoshioka, K. Yoshida, H. Yamazaki, N. Nonomura and K. Ogawa, "The emerging role of high-dose-rate (HDR) brachytherapy as monotherapy for prostate cancer," Journal of radiation research **54**, 781-788 (2013).

67. P. Hoskin, A. Rojas, P. Ostler, R. Hughes, R. Alonzi, G. Lowe and L. Bryant, "High-dose-rate brachytherapy alone given as two or one fraction to patients for locally advanced prostate cancer: acute toxicity," Radiotherapy and oncology : journal of the European Society for Therapeutic Radiology and Oncology **110**, 268-271 (2014).

68. P. J. Prada, J. Cardenal, A. G. Blanco, J. Anchuelo, M. Ferri, G. Fernandez, E. Arrojo, A. Vazquez, M. Pacheco and J. Fernandez, "High-dose-rate interstitial brachytherapy as monotherapy in one fraction for the treatment of favorable stage prostate cancer: Toxicity and long-term biochemical results," Radiotherapy and oncology : journal of the European Society for Therapeutic Radiology and Oncology **119**, 411-416 (2016).

69. G. Morton, H. T. Chung, M. McGuffin, J. Helou, L. D'Alimonte, A. Ravi, P. Cheung, E. Szumacher, S. Liu, M. Al-Hanaqta, L. Zhang, A. Mamedov and A. Loblaw, "Prostate high dose-rate brachytherapy as monotherapy for low and intermediate risk prostate cancer: Early toxicity and quality-of life results from a randomized phase II clinical trial of one fraction of 19Gy or two fractions of 13.5Gy," Radiotherapy and oncology : journal of the European Society for Therapeutic Radiology and Oncology **122**, 87-92 (2017).

70. H. Hauswald, M. R. Kamrava, J. M. Fallon, P. C. Wang, S. J. Park, T. Van, L. Borja, M. L. Steinberg and D. J. Demanes, "High-Dose-Rate Monotherapy for Localized Prostate Cancer: 10-Year Results," International journal of radiation oncology, biology, physics **94**, 667-674 (2016).

71. M. Dattoli, K. Wallner, L. True, J. Cash and R. Sorace, "Long-term outcomes after treatment with brachytherapy and supplemental conformal radiation for prostate cancer patients having intermediate and high-risk features," Cancer **110**, 551-555 (2007).

72. B. R. Pieters, E. Rezaie, E. D. Geijsen, K. Koedooder, J. N. van der Grient, L. E. Blank, T. M. de Reijke and C. C. Koning, "Development of late toxicity and International Prostate Symptom Score resolution after external-beam radiotherapy combined with pulsed dose rate brachytherapy for prostate cancer," International journal of radiation oncology, biology, physics **81**, 758-764 (2011).

73. S. Lettmaier, M. Lotter, S. Kreppner, A. Strnad, R. Fietkau and V. Strnad, "Long term results of a prospective dose escalation phase-II trial: interstitial pulsed-dose-rate brachytherapy as boost for intermediate- and high-risk prostate cancer," Radiotherapy and oncology : journal of the European Society for Therapeutic Radiology and Oncology **104**, 181-186 (2012).

74. A. A. Martinez, G. Gustafson, J. Gonzalez, E. Armour, C. Mitchell, G. Edmundson, W. Spencer, J. Stromberg, R. Huang and F. Vicini, "Dose escalation using conformal high-dose-rate brachytherapy improves outcome in unfavorable prostate cancer," International journal of radiation oncology, biology, physics **53**, 316-327 (2002).

75. D. J. Demanes, R. R. Rodriguez, L. Schour, D. Brandt and G. Altieri, "High-dose-rate intensity-modulated brachytherapy with external beam radiotherapy for prostate cancer: California endocurietherapy's 10-year results," International journal of radiation oncology, biology, physics **61**, 1306-1316 (2005).

76. S. Deger, D. Boehmer, J. Roigas, T. Schink, K. D. Wernecke, T. Wiegel, W. Hinkelbein, V. Budach and S. A. Loening, "High dose rate (HDR) brachytherapy with conformal radiation therapy for localized prostate cancer," European urology **47**, 441-448 (2005).

77. T. Akimoto, K. Ito, J. Saitoh, S. E. Noda, K. Harashima, H. Sakurai, Y. Nakayama, T. Yamamoto, K. Suzuki, T. Nakano and H. Niibe, "Acute genitourinary toxicity after high-dose-rate (HDR) brachytherapy combined with hypofractionated external-beam radiation therapy for localized prostate cancer: correlation between the urethral dose in HDR brachytherapy and the severity of acute genitourinary toxicity," International journal of radiation oncology, biology, physics **63**, 463-471 (2005).

78. P. J. Hoskin, K. Motohashi, P. Bownes, L. Bryant and P. Ostler, "High dose rate brachytherapy in combination with external beam radiotherapy in the radical treatment of prostate cancer: initial results of a randomised phase three trial," Radiotherapy and oncology : journal of the European Society for Therapeutic Radiology and Oncology **84**, 114-120 (2007).

79. P. J. Hoskin, A. M. Rojas, P. J. Bownes, G. J. Lowe, P. J. Ostler and L. Bryant, "Randomised trial of external beam radiotherapy alone or combined with high-dose-rate brachytherapy boost for localised prostate cancer," Radiotherapy and oncology : journal of the European Society for Therapeutic Radiology and Oncology **103**, 217-222 (2012).

80. P. J. Hoskin, A. Colombo, A. Henry, P. Niehoff, T. Paulsen Hellebust, F. A. Siebert and G. Kovacs, "GEC/ESTRO recommendations on high dose rate afterloading brachytherapy for localised prostate cancer: an update," Radiotherapy and oncology : journal of the European Society for Therapeutic Radiology and Oncology **107**, 325-332 (2013).

81. J. Mohler, R. R. Bahnson, B. Boston, J. E. Busby, A. D'Amico, J. A. Eastham, C. A. Enke, D. George, E. M. Horwitz, R. P. Huben, P. Kantoff, M. Kawachi, M. Kuettel, P. H. Lange, G. Macvicar, E. R. Plimack, J. M. Pow-Sang, M. Roach, 3rd, E. Rohren, B. J. Roth, D. C. Shrieve, M. R. Smith, S. Srinivas, P. Twardowski and P. C. Walsh, "NCCN clinical practice guidelines in oncology: prostate cancer," Journal of the National Comprehensive Cancer Network : JNCCN **8**, 162-200 (2010).

82. C. E. Vargas, A. A. Martinez, T. P. Boike, W. Spencer, N. Goldstein, G. S. Gustafson, D. J. Krauss and J. Gonzalez, "High-dose irradiation for prostate cancer via a high-dose-rate brachytherapy boost: results of a phase I to II study," International journal of radiation oncology, biology, physics **66**, 416-423 (2006).

83. R. M. Galalae, G. Kovacs, J. Schultze, T. Loch, P. Rzehak, R. Wilhelm, H. Bertermann, B. Buschbeck, P. Kohr and B. Kimmig, "Long-term outcome after elective irradiation of the pelvic lymphatics and local dose escalation using high-dose-rate brachytherapy for locally advanced prostate cancer," International journal of radiation oncology, biology, physics **52**, 81-90 (2002).

84. S. P. Elliott, M. V. Meng, E. P. Elkin, J. W. McAninch, J. Duchane, P. R. Carroll and P. I. Ca, "Incidence of urethral stricture after primary treatment for prostate cancer: data From CaPSURE," The Journal of urology **178**, 529-534; discussion 534 (2007).

85. R. C. Chen, J. A. Clark and J. A. Talcott, "Individualizing quality-of-life outcomes reporting: how localized prostate cancer treatments affect patients with different levels of baseline urinary, bowel, and sexual function," Journal of clinical oncology : official journal of the American Society of Clinical Oncology **27**, 3916-3922 (2009).

86. M. G. Sanda, R. L. Dunn, J. Michalski, H. M. Sandler, L. Northouse, L. Hembroff, X. Lin, T. K. Greenfield, M. S. Litwin, C. S. Saigal, A. Mahadevan, E. Klein, A. Kibel, L. L. Pisters, D. Kuban, I. Kaplan, D. Wood, J. Ciezki, N. Shah and J. T. Wei, "Quality of life and satisfaction with outcome among prostate-cancer survivors," The New England journal of medicine **358**, 1250-1261 (2008).

87. J. L. Stanford, Z. Feng, A. S. Hamilton, F. D. Gilliland, R. A. Stephenson, J. W. Eley, P. C. Albertsen, L. C. Harlan and A. L. Potosky, "Urinary and sexual function after radical prostatectomy for clinically localized prostate cancer: the Prostate Cancer Outcomes Study," Jama **283**, 354-360 (2000).

88. M. J. Zelefsky, E. J. Levin, M. Hunt, Y. Yamada, A. M. Shippy, A. Jackson and H. I. Amols, "Incidence of late rectal and urinary toxicities after three-dimensional conformal radiotherapy and intensity-modulated radiotherapy for localized prostate cancer," International journal of radiation oncology, biology, physics **70**, 1124-1129 (2008).

89. A. Heidenreich, J. Bellmunt, M. Bolla, S. Joniau, M. Mason, V. Matveev, N. Mottet, H. P. Schmid, T. van der Kwast, T. Wiegel, F. Zattoni and U. European Association of, "EAU guidelines on prostate cancer. Part 1: screening, diagnosis, and treatment of clinically localised disease," European urology **59**, 61-71 (2011).

90. V. A. Moyer and U. S. P. S. T. Force, "Screening for prostate cancer: U.S. Preventive Services Task Force recommendation statement," Annals of internal medicine **157**, 120-134 (2012).

91. N. Mohammed, L. Kestin, M. Ghilezan, D. Krauss, F. Vicini, D. Brabbins, G. Gustafson, H. Ye and A. Martinez, "Comparison of acute and late toxicities for three modern high-dose radiation treatment techniques for localized prostate cancer," International journal of radiation oncology, biology, physics **82**, 204-212 (2012).

92. A. R. Mundy and D. E. Andrich, "Posterior urethral complications of the treatment of prostate cancer," BJU international **110**, 304-325 (2012).

93. S. V. Dandapani and M. G. Sanda, "Measuring health-related quality of life consequences from primary treatment for early-stage prostate cancer," Seminars in radiation oncology **18**, 67-72 (2008).

94. G. S. Merrick, W. M. Butler, K. E. Wallner, R. W. Galbreath, R. L. Anderson, Z. A. Allen and E. Adamovich, "Risk factors for the development of prostate brachytherapy related urethral strictures," The Journal of urology **175**, 1376-1380; discussion 1381 (2006).

95. B. R. Hindson, J. L. Millar and B. Matheson, "Urethral strictures following high-dose-rate brachytherapy for prostate cancer: analysis of risk factors," Brachytherapy **12**, 50-55 (2013).

96. L. Sullivan, S. G. Williams, K. H. Tai, F. Foroudi, L. Cleeve and G. M. Duchesne, "Urethral stricture following high dose rate brachytherapy for prostate cancer," Radiotherapy and oncology : journal of the European Society for Therapeutic Radiology and Oncology **91**, 232-236 (2009).

97. D. R. Zwahlen, N. Andrianopoulos, B. Matheson, G. M. Duchesne and J. L. Millar, "High-dose-rate brachytherapy in combination with conformal external beam radiotherapy in the treatment of prostate cancer," Brachytherapy **9**, 27-35 (2010).

98. M. J. Zelefsky, H. Chan, M. Hunt, Y. Yamada, A. M. Shippy and H. Amols, "Long-term outcome of high dose intensity modulated radiation therapy for patients with clinically localized prostate cancer," The Journal of urology **176**, 1415-1419 (2006).

99. V. Fonteyne, G. Villeirs, N. Lumen and G. De Meerleer, "Urinary toxicity after high dose intensity modulated radiotherapy as primary therapy for prostate cancer," Radiotherapy and oncology : journal of the European Society for Therapeutic Radiology and Oncology **92**, 42-47 (2009).

100. H. Ishiyama, M. Kitano, T. Satoh, S. Kotani, M. Uemae, K. Matsumoto, H. Okusa, K. Tabata, S. Baba and K. Hayakawa, "Genitourinary toxicity after high-dose-rate (HDR) brachytherapy combined with Hypofractionated External beam radiotherapy for localized prostate cancer: an analysis to determine the correlation between dose-volume histogram parameters in HDR brachytherapy and severity of toxicity," International journal of radiation oncology, biology, physics **75**, 23-28 (2009).

101. I. C. Hsu, K. Bae, K. Shinohara, J. Pouliot, J. Purdy, G. Ibbott, J. Speight, E. Vigneault, R. Ivker and H. Sandler, "Phase II trial of combined high-dose-rate brachytherapy and external beam radiotherapy for adenocarcinoma of the prostate: preliminary results of RTOG 0321," International journal of radiation oncology, biology, physics **78**, 751-758 (2010).

102. G. C. Morton, D. A. Loblaw, H. Chung, G. Tsang, R. Sankreacha, A. Deabreu, L. Zhang, A. Mamedov, P. Cheung, D. Batchelar, C. Danjoux and E. Szumacher, "Health-related quality of life after single-fraction high-dose-rate brachytherapy and hypofractionated external beam radiotherapy for prostate cancer," International journal of radiation oncology, biology, physics **80**, 1299-1305 (2011).

103. P. Ghadjar, T. Keller, C. A. Rentsch, B. Isaak, F. Behrensmeier, A. Stroux, G. N. Thalmann and D. M. Aebersold, "Toxicity and early treatment outcomes in low- and intermediate-risk prostate cancer managed by high-dose-rate brachytherapy as a monotherapy," Brachytherapy **8**, 45-51 (2009).

104. B. A. Erickson, J. W. McAninch, M. L. Eisenberg, S. L. Washington and B. N. Breyer, "Management for prostate cancer treatment related posterior urethral and bladder neck stenosis with stents," The Journal of urology **185**, 198-203 (2011).

105. J. J. Meeks, S. B. Brandes, A. F. Morey, M. Thom, N. Mehdiratta, C. Valadez, M. A. Granieri and C. M. Gonzalez, "Urethroplasty for radiotherapy induced bulbomembranous strictures: a multi-institutional experience," The Journal of urology **185**, 1761-1765 (2011).

106. A. S. Glass, J. W. McAninch, U. B. Zaid, N. M. Cinman and B. N. Breyer, "Urethroplasty after radiation therapy for prostate cancer," Urology **79**, 1402-1405 (2012).

107. P. Grimm, I. Billiet, D. Bostwick, A. P. Dicker, S. Frank, J. Immerzeel, M. Keyes, P. Kupelian, W. R. Lee, S. Machtens, J. Mayadev, B. J. Moran, G. Merrick, J. Millar, M. Roach, R. Stock, K. Shinohara, M. Scholz, E. Weber, A. Zietman, M. Zelefsky, J. Wong, S. Wentworth, R. Vera and S. Langley, "Comparative analysis of prostate-specific antigen free survival outcomes for patients with low, intermediate and high risk prostate cancer treatment by radical therapy. Results from the Prostate Cancer Results Study Group," BJU international **109 Suppl 1**, 22-29 (2012).

108. A. A. Martinez, J. Gonzalez, H. Ye, M. Ghilezan, S. Shetty, K. Kernen, G. Gustafson, D. Krauss, F. Vicini and L. Kestin, "Dose escalation improves cancer-related events at 10 years for intermediate- and high-risk prostate cancer patients treated with hypofractionated high-dose-rate boost and external beam radiotherapy," International journal of radiation oncology, biology, physics **79**, 363-370 (2011).

109. A. Tewari, J. Peabody, R. Sarle, G. Balakrishnan, A. Hemal, A. Shrivastava and M. Menon, "Technique of da Vinci robot-assisted anatomic radical prostatectomy," Urology **60**, 569-572 (2002).

110. J. B. Malcolm, M. D. Fabrizio, B. B. Barone, R. W. Given, R. S. Lance, D. F. Lynch, J. W. Davis, M. E. Shaves and P. F. Schellhammer, "Quality of life after open or robotic prostatectomy, cryoablation or brachytherapy for localized prostate cancer," The Journal of urology **183**, 1822-1828 (2010).

111. N. Tselis, U. W. Tunn, G. Chatzikonstantinou, N. Milickovic, D. Baltas, M. Ratka and N. Zamboglou, "High dose rate brachytherapy as monotherapy for localised prostate cancer: a hypofractionated two-implant approach in 351 consecutive patients," Radiation oncology **8**, 115 (2013).

112. M. A. Ebert, "Possibilities for intensity-modulated brachytherapy: technical limitations on the use of non-isotropic sources," Physics in medicine and biology **47**, 2495-2509 (2002).

113. M. A. Ebert, "Potential dose-conformity advantages with multi-source intensity-modulated brachytherapy (IMBT)," Australasian physical & engineering sciences in medicine / supported by the Australasian College of Physical Scientists in Medicine and the Australasian Association of Physical Sciences in Medicine **29**, 165-171 (2006).

114. M. J. Webster, S. Devic, T. Vuong, D. Y. Han, D. Scanderbeg, D. Choi, B. Song and W. Y. Song, "HDR brachytherapy of rectal cancer using a novel grooved-shielding applicator design," Medical physics **40**, 091704 (2013).

115. L. Lin, R. R. Patel, B. R. Thomadsen and D. L. Henderson, "The use of directional interstitial sources to improve dosimetry in breast brachytherapy," Medical physics **35**, 240-247 (2008).

116. Q. E. Adams, J. Xu, E. K. Breitbach, X. Li, S. A. Enger, W. R. Rockey, Y. Kim, X. Wu and R. T. Flynn, "Interstitial rotating shield brachytherapy for prostate cancer," Medical physics **41**, 051703 (2014).

117. J. Skowronek, "Brachytherapy in the therapy of prostate cancer - an interesting choice," Contemporary oncology **17**, 407-412 (2013).

118. S. A. Enger, D. R. Fisher and R. T. Flynn, "Gadolinium-153 as a brachytherapy isotope," Physics in medicine and biology **58**, 957-964 (2013).

119. D. J. Krauss, H. Ye, A. A. Martinez, B. Mitchell, E. Sebastian, A. Limbacher and G. S. Gustafson, "Favorable Preliminary Outcomes for Men With Low- and Intermediate-risk Prostate Cancer Treated With 19-Gy Single-fraction High-dose-rate Brachytherapy," International journal of radiation oncology, biology, physics **97**, 98-106 (2017).

120. A. Okabe, *Spatial tessellations : concepts and applications of Voronoi diagrams*, 2nd ed. (Wiley, Chichester ; New York, 2000).

121. E. C. White, M. R. Kamrava, J. Demarco, S. J. Park, P. C. Wang, O. Kayode, M. L. Steinberg and D. J. Demanes, "High-dose-rate prostate brachytherapy consistently results in high quality dosimetry," International journal of radiation oncology, biology, physics **85**, 543-548 (2013).